Journal Pre-proof

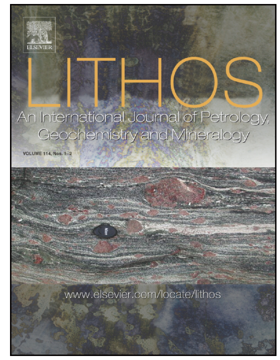

The composition of amphibole phenocrysts in Neogene mafic volcanic rocks from the Puna plateau: Insights on the evolution of hydrous back-arc magmas

Guadalupe Maro, Robert B. Trumbull, Pablo J. Caffe, Cynthia B. Jofré, Rubén Filipovich, Daniel A. Frick

PII: S0024-4937(20)30375-3

DOI: https://doi.org/10.1016/j.lithos.2020.105738

Reference: LITHOS 105738

To appear in: *LITHOS*

Received date: 25 October 2019

Revised date: 6 August 2020

Accepted date: 7 August 2020

Please cite this article as: G. Maro, R.B. Trumbull, P.J. Caffe, et al., The composition of amphibole phenocrysts in Neogene mafic volcanic rocks from the Puna plateau: Insights on the evolution of hydrous back-arc magmas, *LITHOS* (2020), https://doi.org/10.1016/j.lithos.2020.105738

This is a PDF file of an article that has undergone enhancements after acceptance, such as the addition of a cover page and metadata, and formatting for readability, but it is not yet the definitive version of record. This version will undergo additional copyediting, typesetting and review before it is published in its final form, but we are providing this version to give early visibility of the article. Please note that, during the production process, errors may be discovered which could affect the content, and all legal disclaimers that apply to the journal pertain.

© 2020 Published by Elsevier.

Journal Pre-proof

The composition of amphibole phenocrysts in Neogene mafic volcanic rocks from the Puna plateau: insights on the evolution of hydrous back-arc magmas.

Guadalupe Maro[1*], Robert B. Trumbull[3], Pablo J. Caffe[1], Cynthia B. Jofré[1], Rubén Filipovich[2], and Daniel A. Frick[3]

[1] Instituto de Ecorregiones Andinas (INECOA), Universidad Nacional de Jujuy - CONICET, Instituto de Geología y Minería, Av. Bolivia 1661, San Salvador de Jujuy (CP 4600), Jujuy, Argentina.

[2] Instituto de Bio y Geociencias del Noroeste Argentino (UNSa-CONICET), 9 de Julio 14, 4405 Rosario de Lerma, Salta, Argentina.

[3] GFZ German Research Centre for Geosciences, Telegrafenberg 14473, Potsdam, Germany.

*Corresponding author: Guadalupe Maro. Tel.:+543884221593, E-mail address: maroguadalupe@gmail.com

KEY WORDS: amphibole, trace elements, thermobarometry, copper, Altiplano-Puna Magma Body

ABSTRACT

In typical Andean arc magmas, amphibole appears as a phenocryst phase only after considerable differentiation. However, some near-primitive volcanic rocks (high-Mg andesites and basalts) from monogenetic centers in the Puna plateau of Argentina also contain amphibole phenocrysts, implying special conditions of hydrous magma generation in this back-arc setting. This study documents typical examples from Southern and Northern Puna regions and uses the major and trace-element compositions of amphibole to constrain a petrogenetic model for the hydrous magmas.

There are significant differences in the nature of amphiboles and their host lavas depending on location of the volcanic centers in the Southern and the Northern Puna regions. In the Southern Puna, basaltic andesitic lavas have Sr/Y values > 40 and amphiboles show skeletal forms

Journal Pre-proof

and occur in an assemblage with olivine and pyroxene. The amphibole compositions are relatively Al- and Ti-poor compared to the Northern Puna. Thermobarometry indicates amphibole crystallization temperatures of 960-1000 °C at moderate pressure (< 5 kbar). In contrast, the mafic lavas from centers in the Northern Puna show Sr/Y ratios lower than 20 and amphiboles in these rocks coexist with a plagioclase-orthopyroxene assemblage. The Northern Puna amphiboles have higher Ti and Al contents than those in the southern region and the thermobarometry estimates imply generally higher crystallization temperatures (>1000 °C) and pressures (6-8 kbar). Furthermore, the chemical composition of amphibole phenocrysts in the Northern Puna Campo Negro center suggests an alkaline affinity of the parental magmas which, together with radiogenic isotope data from earlier studies, indicates a significant contribution of the enriched lithosphere in the magma source.

The new data collectively suggest high pressure evolution of hydrous magmas in the Southern Puna, whereas the Northern Puna magmas underwent more differentiation at higher levels in the crust. This contrast in the evolution history of magmas below both regions can be connected with their position relative to partial melting zones in the mid-upper crust, which are larger and longer-lived in the north than in the south, thus favoring a slower ascent of magmas in that region.

INTRODUCTION

Monogenetic mafic volcanism in the Puna plateau is of great importance because its products are close representative for primary, mantle-derived magmatism in this region (Kay et al., 1994; Risse et al., 2013; Ducea et al. 2013; Murray et al., 2015; Maro et al., 2017a). They provide an estimate for one of the fundamental "ingredients" needed to form the hybrid silicic andesite to dacitic magmas that dominate the Central Volcanic Zone (CVZ). The main geological and compositional features of mafic volcanism in the Puna region have been documented in the cited studies. One of those general features is a lack of hydrous phases in the phenocryst assemblage of the most

Journal Pre-proof

primitive rocks (trachybasalts, basalts, high-Mg basaltic andesites and trachy-basaltic andesites). Amphibole phenocrysts typically occur in the compositionally more evolved andesitic and dacitic rocks. For example, the study of basaltic andesite to dacite rocks from 12 volcanic centers in the western Cordillera by Trumbull et al. (1999) found primary amphibole only in samples with more than 58 wt.% SiO_2. However, there are exceptional cases of amphibole-bearing mafic lavas with chemical properties close to primitive magmas (e.g., high Ni and Cr contents, high Mg#). Most of them classify as Mg-rich basaltic andesites and andesites, but amphibole-bearing basalt is also known as enclaves in andesite from the Cerro Negro center, Northern Puna (Presta and Caffe, 2014). The implication of amphibole in these near-primitive rocks is that the parental magmas were hydrous, which is unusual for the otherwise "dry" back-arc setting. None of the localities was documented in detail before, which motivated the study presented here. Samples were investigated from three monogenetic centers, two in the Southern Puna (Pasto Ventura field and Carachipampa complex), and one (Campo Negro) in the Northern Puna (Fig. 1). Important for the regional context of this study are the detailed geochemical-petrogenetic studies on the mafic magmatism in the Southern and Northern Puna regions (see below), as well as geophysical data that constrain crustal thickness and density variations in the two regions (Yuan et al., 2002; McGlashan et al. 2008).

We present detailed petrographic descriptions and bulk-rock geochemical analyses of the amphibole-bearing mafic lavas, as well as the major-element composition of the amphiboles and associated phenocryst phases. These data are the basis for themobarometric estimates to crystallization conditions. In-situ trace element analyses of amphibole constitute the first data of this kind for the Neogene magmatism in the Puna. The combined information is used to constrain the origin of hydrous mafic magmatism in the southern and northern segments of the Puna plateau and to assess differences between them.

The recognition of hydrous mafic magmas with amphibole phenocrysts in the Central Andes is potentially important to the question of Cu endowment in arc magmas and their role in formation of porphyry Cu deposits. Theoretical studies suggest the importance of deep-level magma generation (thick crust, high Sr/Y ratios) with significant initial water contents and particular conditions of magma storage and evolution in the crust (e.g. Chiaradia and Caricchi, 2017; Lee and Tang, 2020). The volcanic centers featured here are not mineralized and they are younger than the known Cu deposits from the region. Nevertheless, these rocks are possible proxies for the hydrous, mafic precursor magmas postulated for the porphyry systems in the Central Andes backarc but rarely, if ever, observed (e.g., Halter et al., 2004; Mazzuoli et al., 2008; Stremel, 2016). Therefore, we also determined the copper concentrations in the amphibole phenocrysts and discuss the results in terms of magmatic Cu contents and their potential significance for understanding Cu mineralized systems in the Puna region.

GEOLOGICAL BACKGROUND

The Puna (22°S - 26°S) is a wide, arid, area of high elevation that develops, together with the Altiplano of Bolivia and Peru, the Central Andean Plateau. The Puna is divided into a Northern and Southern region based on the different geologic characteristics recognized between them (Alonso and Viramonte, 1987). The two are delimited by the Calama-Olacapato-El Toro lineament, a master structure that is transverse to the N-S oriented volcanic arc and the main thrust faults (Fig. 1). Differences between these regions include crustal thickness, which attains its minimum in the Northern Puna and Altiplano plateau (~ 45 km) and is up to 20 km thicker in the Southern Puna (Yuan et al., 2002; McGlashan et al. 2008). Other variations of the Puna plateau from north to south are an increase of the average elevation, a lessening of the subduction angle, and changes in the geology of the pre-Andean basement from early Paleozoic sedimentary sequences in the north to igneous and high-grade metamorphic basement in the south (Allmendinger et al., 1997; Yuan et al., 2002; Heit et al., 2008; Prezzi et al., 2009).

Neogene volcanic units are widespread in both the Southern and Northern Puna regions, where they form andesitic to dacitic stratovolcanoes and silicic domes (Coira et al., 1993; Caffe et al., 2002), extensive and voluminous high-K dacitic and minor rhyolitic ignimbrites (e.g., Kay et al., 2010), and monogenetic mafic centers (Risse et al., 2013; Guzmán et al., 2006; Maro and Caffe, 2016; 2017). A particular feature of Neogene volcanism is the presence of one of the largest caldera-sourced ignimbrite provinces in the world: the Altiplano-Puna Volcanic Complex or APVC (de Silva, 1989; Kay et al., 2010; Salisbury et al., 2010), that occupies extensive areas in the Northern Puna and Southern Bolivian Altiplano.

The Puna plateau has been well studied geophysically, and these studies have documented a mid-crustal zone with low seismic velocity and high electrical conductivity beneath the APVC which is suggested to represent an active zone of partial melting (Chmielowski et al., 1999; Zandt et al., 2003; Schilling et al., 2006; Ward et al., 2014). This is referred to as the Altiplano-Puna Magma Body or APMB. A similar geophysical anomaly is found in the Southern Puna near the Cerro Galán caldera complex, but it is smaller and deeper, being located in the lower crust and upper mantle (Ward et al., 2014; Beck et al., 2015). Seismic tomography images of the mantle wedge beneath the Central Andes show a complex velocity distribution, which many workers attributed to lithosphere delamination and upwelling of asthenosphere (e.g., Schurr et al., 2006; Bianchi et al., 2013). The role of lithosphere delamination as a trigger of the Puna back arc magmatism is a widely accepted hypothesis (Kay et al., 1994; Risse et al., 2013; Murray et al., 2015; Maro et al., 2017a), although there are differences of opinion on the mantle source that was the major contributor to partial melting (e.g., Murray et al., 2015 vs. Maro et al., 2017a).

The Puna plateau and adjacent parts of the Eastern Cordillera and northernmost Pampean Ranges are host to several Cu (±Mo, ±Au) porphyry deposits and occurrences (e.g., Taca-Taca, Inca Viejo, Las Burras, Pancho Arias, Río Grande, Bajo de la Alumbrera; see Fig. 1). These are related to Miocene intermediate to silicic magmatism (Sillitoe, 1977; Kay et al., 1999; Stremel, 2016).

Neogene monogenetic volcanism and features of the amphibole-bearing centers

The Neogene mafic volcanism in the Puna region comprises monogenetic volcanoes of small size that occur either as isolated centers or as clusters which form larger volcanic fields, the latter type being more numerous in the Southern Puna than in the north (Maro and Caffe, 2017; Báez et al., 2017; Maro et al., 2017b; Filipovich et al., 2019). Another contrast between these two regions is that the age of volcanism is somewhat younger in the south than in the north (Pliocene-Holocene vs. Upper Miocene-Lower Pliocene, respectively) (Kay et al., 1994; Risse et al., 2008; Maro and Caffe, 2017), where centers are notably more eroded (Maro and Caffe, 2017). The Southern Puna centers of interest in this paper, Pasto Ventura and Carachipampa, formed over a time span between at least ~0.75 and ~0.27 Ma (Risse et al., 2008; Zhou et al., 2013). The Northern Puna Campo Negro center has not been dated directly, but its age is constrained to be late Miocene to early Pliocene based on an overlying ignimbrite that correlates with pyroclastic deposits of the Convento-Coyaguayma volcano (Seggiaro, 1994). Those deposits are between about 6.5 and 2 Ma based on the underlying Las Termas Ignimbrite (6.45 ± 0.15 Ma: Seggiaro, 1994) and the overlying lava of the Campanario volcano (2.03 ± 0.07 Ma: Aquater, 1979).

The products of Puna mafic volcanism in both the Southern Puna and Northern Puna regions are mostly olivine + clinopyroxene- or orthopyroxene-bearing lavas that classify as calc-alkaline basaltic andesites and high-MgO andesites; basaltic and shoshonitic compositions are less common (Risse et al., 2013; Maro et al., 2017a). Amphibole-bearing mafic lavas are extremely rare in the Puna. Effectively, up to now, only mafic volcanic rocks collected from Pasto Ventura and Carachipampa localities in the Southern Puna and from Campo Negro in the Northern Puna (Fig. 1) have been found to contain amphibole as an important modal component of the lavas.

The Pasto Ventura volcanic field (26°43.7’S-67°12.5’W) is represented mainly by clustered small-volume, basaltic (basaltic andesite) features including scoria cones, domes, maars and tuff rings (Fig. 1) (Filipovich et al., 2019). The Carachipampa complex (26°34.3’S-67°26.5’W) consists of a cluster of lava flows, lava domes and superimposed, eroded scoria cones (Fig. 1). These volcanic structures are associated with a variability of eruptive styles such as effusive, Hawaiian, Strombolian, violent Strombolian and phreatomagmatic (Filipovich et al., 2019). Domes are flat-topped and roughly circular (commonly named *tortas*) or *coulèes*. All the volcanic products have slight compositional difference from basaltic andesite to basaltic trachyandesite to trachyandesite (Filipovich et al., 2019). In thin section, lavas associated with scoria cones have a porphyritic vesicular texture with phenocrysts of anhydrous minerals only, whereas the lava domes show porphyritic texture with ubiquitous clinopyroxene and variable amounts of orthopyroxene, olivine and amphibole phenocrysts embedded in an intersertal to pilotaxitic groundmass. A common feature of the Pasto Ventura samples is the presence of quartz xenocrysts showing embayments rimmed with clinopyroxene.

The Campo Negro eruptive center (23°3.6’S-66°38.8’W), in the Northern Puna, is a solitary, highly eroded scoria cone of 150 m in diameter and 20 m high, from which at least 4 andesitic flows extend toward the southeast, north, east and northeast (Fig. 1). The lavas contain phenocrysts of amphibole, plagioclase, two pyroxenes and oxides in a pilotaxitic groundmass. A unique feature of the Campo Negro center compared to the other monogenetic volcanoes from the Northern or Southern Puna, is the presence of amphibole-bearing basaltic enclaves up to 3 cm long (Presta and Caffe, 2014).

METHODOLOGY

Bulk-rock major and trace element concentrations were obtained by X-ray fluorescence (XRF) in the Instituto de Geología y Minería, Universidad Nacional de Jujuy (Argentina), using a Rigaku FX2000 spectrometer with a Rh tube operated at 50 kV and 45 mA. Ground and homogenized rock powders were fused with a lithium tetraborate flux for major element analyses. Trace elements Ba, Sr, Rb, Zr, Nb, Hf, Y, Th, and U were analyzed on pressed powder discs with a methyl methacrylate binder. The XRF intensities were converted to concentrations using reference standards from the US Geological Survey and the Japanese Geological Survey. Other trace and rare earth elements (REE) were determined in a selection of 11 samples by lithium metaborate/tetraborate fusion and ICP-MS analysis in the ALS-Chemical laboratories. Samples were fused, diluted and analyzed by Perkin Elmer Sciex ELAN 6000, 6100 or 9000 ICP/MS. Three blanks and five analyses of control standards (three before the sample group and two after) were analyzed per group of samples. The whole rock geochemistry data for the CN09 (Campo Negro) samples were previously presented in Maro et al. (2017a), except for Cu analysis. The full geochemical data set is given in Table 1.

Mineral compositions were determined *in situ* on polished thin sections (thickness 100 μm) of a selection of 7 samples using a JEOL JXA-8230 electron microprobe at the GFZ Potsdam, employing wavelength dispersive spectrometers. The microprobe was operated at 15 kV accelerating voltage and a beam current of 15 nA, with a fully- focused (ca. 1 micron) beam for clinopyroxene and olivine. Plagioclase was analyzed using a defocused 5 micron beam and Na was measured first in the sequence to minimize alkali loss. The conversion of measured intensities to concentrations was based on natural and synthetic mineral standards after correction using the PAP method (Pouchou & Pichoir, 1987). Amphibole classification was defined following the recommendations of the International Mineralogical Association (IMA) described in Leake et al. (1997) for microprobe data, based on a general formula $AB_2{}^{VI}C_5{}^{IV}T_8O_{22}(OH)_2$, and using the Excel spreadsheet of Ridolfi et al. (2010). Given the uncertainty about the H_2O and halogen contents, the mineral formulae were calculated on a 23-oxygen-atom basis assuming 2(OH, F, Cl) (Leake et al., 1997).

In situ trace element concentration in amphibole, plagioclase and pyroxene were analyzed by laser ablation inductively coupled plasma mass spectrometry (LA- ICP-MS) at the GFZ Potsdam, using 3 of the same polished thin sections as for EMPA analyses. The instrument is a custom-built deep-UV (196 nm) femtosecond laser ablation (fsLA) system (GFZ fem2), comprising a frequency-quadrupled Spectra Physics Solstice femtosecond laser (see Schuessler and von Blanckenburg, 2014, for technical details). The aerosol was transported into the ICP-MS (Thermo Fisher Scientific iCAP) using helium as carrier gas. The fsLA beam has a Gaussian energy distribution, thus the laser beam (ca. 28 µm in diameter) is continuously scanned over a small area (50x100 µm) on the samples rather than a single spot analysis. ICP-MS and fsLA were tuned daily for highest sensitivity, while maintaining a $^{238}U/^{232}Th$ ratio on NIST SRM610 close to 1 and $^{232}Th^{16}O/^{232}Th$ below 0.7%. Instrument settings for fsLA and ICP-MS are reported in Supplementary Data Electronic Appendix (Table S1). Data evaluation for chemical composition analysis was carried out in StalQuant, a Python-based program developed at the ETH Zürich (Fricker, 2012) and modified to allow direct import of iCAP-Qc data. NIST SRM610 was used as the external standard, while differences in the ablation yield were corrected using a 100% weight oxide approach (Liu et al., 2008). Reference values for standard reference materials were taken from Jochum et al. (2011) and the GeoReM database (Jochum et al., 2005). Uncertainty for the elements is estimated from repeated determination of NIST612, BHVO-2G, ATHO-G, ML3B-G, and GOR132-G. Results not reported were below the limit of quantification (LOQ) as estimated following Longerich et al. (1996). Representative results of mineral compositions are shown in Tables 2 and 4, and complete data are given in Supplementary Data Electronic Appendix (Tables S2-S9).

RESULTS

Bulk-rock geochemistry

Journal Pre-proof

The lavas from the Southern Puna centers Carachipampa (C) and Pasto Ventura (PV), and those from Campo Negro (CN) in the Northern Puna classify as high-K calc-alkaline andesites (Fig. 2A and B) with a narrow range of SiO_2 (57-59 wt.%) and 5 to 6 wt.% MgO (Table 1). The samples from all centers overlap on the total alkali-silica diagram (Fig. 2B) but those from the Southern Puna centers (C, PV) have higher alkali contents and plot close to the trachyandesitic field while some samples from the Northern center CN plot in the basaltic andesite field. All samples have high magnesium numbers [Mg# = 100*Mg/(Mg + Fe)] (> 60) and can be classified as Mg-andesites (Wood and Turner, 2009). Moreover, their Ni (50-140 μg/g) and/or Cr contents (240–390 μg/g) are in the range of near-primitive mantle-derived magmas (Blatter and Carmichael, 1998; Straub et al., 2008). An exceptional sample, with basaltic composition (Fig. 2) is from enclaves in the Campo Negro lavas. The sample has 50.4 wt.% SiO_2 and 8.9 wt.% MgO, and it shares the high-K calc-alkaline signature of the andesites, plotting at the border to the shoshonite field on Fig. 2A.

The multielement diagram of Fig. 3A shows pronounced negative Nb and Ta anomalies relative to Ba and La, which is typical for arc magmas. Chondrite-normalized rare-earth elements patterns (Fig. 3B) show, in general, higher LREE enrichment with respect to HREE and moderate negative Eu anomalies (Eu/Eu* = 0.6 - 0.7). There are notable differences between rocks from the northern and southern Puna regions. The Southern Puna amphibole bearing samples show lower values of HREE (Fig. 3B), reflected by their high La/Yb_N (23-25) ratios, whereas the Northern Puna mafic rocks have lower La/Yb_N (8-15) values. Another contrast is shown by Sr and Y concentrations. The Southern Puna andesites have higher Sr contents than those from the north (~800- 900 μg/g against <500 μg/g: Fig. 3C), and lower Y contents (20-22 μg/g against 25-35 μg/g: see Fig. 3D). This distinction in Sr and Y values is expressed in contrasting Sr/Y ratios, which are higher in the Southern Puna samples (37-46) compared with samples from the Northern Puna (13-19: see Table 1). The bulk-rock Cu contents in the amphibole-bearing

Journal Pre-proof

southern Puna samples are between 37 and 54 µg/g, compared with 25 µg/g in Campo Negro from the Northern Puna (Table 1). These values are consistent with bulk-rock Cu values for other arc and back arc rocks in the Central Andes (e.g., Deruelle, 1991; ; Trumbull et al., 1999; Drew et al., 2009; Ducea et al., 2013) and with the globally averaged continental crust (30 µg/g, Rudnick and Gao (2003)).

Petrography

Samples from Carachipampa are gray, massive rocks with about 30 vol. % micro- (< 0.5 mm) to phenocrysts (> 0.5 mm) comprising olivine (45%), clinopyroxene (35%) and amphibole (20%). The groundmass is very fine-grained and displays intersertal to pilotaxitic textures. The amphibole (up to 2 mm) is skeletal in shape (Fig 4A) and has thick opaque reaction rims (up to 70 µm thick). Locally, partial resorption of the core was observed in some grains. Olivine and clinopyroxene commonly appear as subhedral crystals. Clinopyroxene grains regularly show moderate to strong resorption in the rims. They can occur in monomineralic grain clusters, locally with fine, acicular microlites of orthopyroxene. Spinel inclusions are common in all the microphenocryst phases.

The Pasto Ventura andesites are poorly vesiculated, gray to reddish rocks, with common textural banding and composed of about 20 vol. % phenocrysts comprising amphibole (80%), clinopyroxene (18%) and orthopyroxene (2%) in an intersertal to pilotaxitic groundmass. Anhedral and partially reabsorbed quartz xenocrysts and xenoliths of quartzite are common, as was reported for olivine-bearing or orthopyroxene-bearing lavas from the Puna (Risse, et al., 2013; Maro and Caffe, 2016; Maro et al., 2017a). The amphibole in these rocks shows a variety of different textures and morphologies. One group (Fig. 4B) forms large skeletal (subhedral to anhedral) crystals up to 3 mm in size that show strong resorption, mainly at the edges, optical and compositional zoning (oscillatory and reverse), and opacitization on rims and along fractures (up to 20 µm) or in the cores. The zoning in some cases indicates multiple cycles of crystal growth and internal resorption. Another group of amphibole comprises homogenous micro- to phenocrysts with thin, very fine grained reaction rims (< 8 µm). Last, a third group involves smaller grains where breakdown textures are pervasive. Clinopyroxene is the most abundant pyroxene. It occurs as euhedral to subhedral microphenocrysts, commonly with skeletal shapes and strongly resorbed margins. The subordinate orthopyroxene grains are also commonly skeletal, locally rimmed by clinopyroxene, but there are also some large, anhedral crystals of orthopyroxene, probably of xenocrystic origin. A characteristic feature of the Pasto Ventura samples is the presence of amphibole rims around orthopyroxene phenocrysts (Fig. 4C) where both minerals have the same composition as the individual phenocrysts.

The Campo Negro lavas are dark gray banded porphyritic rocks which are distinctive because of the common presence of amphibole-rich basaltic enclaves - the only true basalts known in the Northern Puna (Presta and Caffe, 2014; Maro et al., 2017a). Xenoliths of quartzite are also present in these rocks. Microscopically, the CN lavas are characterized by about 25 vol. % phenocrysts comprising orthopyroxene (40%), plagioclase (25%), amphibole (25%) and clinopyroxene (10%). Groundmasses are pilotaxitic to intersertal. Phenocrysts of amphibole (up to 1 mm) are generally subhedral, sub-rounded, and show opacite rims typically around 30 µm thick (Fig. 4D). Plagioclase shows disequilibrium textures including fine resorption and oscillatory zoning. Locally, small inclusions of amphibole are present. The orthopyroxene and clinopyroxene form subhedral, colorless crystals that show resorption at the edges. The first typically occurs in clusters of medium grain size. Both amphibole and orthopyroxene crystals contain spinel inclusions. Amphibole also locally includes relics of orthopyroxene in the cores (Fig. 4E), as described in the Pasto Ventura samples above.

The Campo Negro basaltic enclaves are 3 cm in size on average, rounded and with sharp contacts with the host andesite. They have approximately the same modal composition as the host lava but the phenocrysts are coarser (up to 5 mm) and the groundmass has a higher

Journal Pre-proof

crystallinity and contains more vesicles (Fig. 4F). The amphibole in these mafic enclaves occurs as euhedral and elongated grains. Orthopyroxene is subhedral and contains abundant opaque inclusions, and plagioclase forms euhedral phenocrysts with a very thin reabsorption zone in the interior. The groundmass is characterized by the large amount of opaque microlites.

Mineral compositions

Pyroxene

In all centers where they are present, orthopyroxene is enstatitic in composition ($En_{81-88}Wo_{1-3}$ Fs_{10-16}) and clinopyroxene classifies as augite ($En_{37-52}Wo_{34-47}$ Fs_{8-17}). Almost all crystals analyzed are Mg-rich (Mg# 72 to 88) and show modest Cr contents (up to 0.74 %) (Table 2). In the Carachipampa and Campo Negro samples, both orthopyroxene and clinopyroxene phenocrysts show only weak normal zoning (1 mol % En decrease from core to rim). In the Pasto Ventura samples, clinopyroxene exhibits reverse zoning with an increase of MgO contents from the core outward (Fig 5A).

Trace element concentrations and inter-element ratios in clinopyroxene phenocrysts from the Southern Puna samples (CP and PV) reflect some of the main characteristics shown by bulk-rock compositions. In detail, Sr is moderately high (Supplementary material, Table S3) as well as clinopyroxene REE patterns show slight negative Eu anomalies and modest to strong depletions in HREE (as shown by Nd/Yb=10-20) (Fig. 5B). The trace element distribution patterns are similar to those shown by the clinopyroxene phenocrysts comprised in mafic rocks with anhydrous assemblages from Southern Puna (see Risse et al., 2013), although LREE to MREE are more enriched in the amphibole-bearing andesites (Fig. 5B).

Olivine

Journal Pre-proof

Olivine compositions from Carachipampa andesites show high Fo (Fo_{80-87}) in the cores (Table 2, Supplementary material, Table S4). There is typically a weak normal zonation, i.e. decreasing forsterite component (Fo) toward the rims (2-4 mol % lower Fo). The average olivine core compositions in each sample are at, or close to, equilibrium with the bulk rock based on the experimental $K_D^{Fe/Mg}$ value of ca. 0.3 (e.g., Roeder and Emslie, 1970). Minor constituents in olivine such as CaO and Cr_2O_3 are in 0.10 wt % and 0.02 wt.% respectively (Table 2). High Ni contents (up to around 2700 μg/g) are widespread (Supplementary material, Table S4), and Ni is well-correlated with the Fo content.

Plagioclase

Plagioclase phenocrysts are only present in the Northern Puna Campo Negro rocks, occurring in both the andesite lava and basaltic enclaves. The plagioclase has a bytownitic composition with An_{75} to An_{78} in the cores (andesite) and An_{73} to An_{79} in the enclave (Table 2). The crystals are zoned, with about 5 mol. % higher An content in the rims (Supplementary material, Table S5).

Trace element composition of plagioclase phenocrysts in the basaltic enclave are strongly Sr-rich (~ 1300 μg/g) and also show moderate, and rather variable, Ba contents (140-250 μg/g) (Supplementary material, Table S6). Plagioclase phenocrysts in the host lava were not analyzed for trace elements.

Oxides

Oxide phases are present in the groundmass in all of the samples studied and in many cases they also occur as inclusions in mafic phenocrysts. The groundmass oxides classify as magnetite, like those reported from other Neogene mafic centers in the Puna (Risse et al., 2013; Maro et al., 2017a). Importantly, there are systematic differences in TiO_2 concentration in the groundmass oxide grains from the different centers: 4-7 wt.% in Carachipampa, 10-17 wt.% in Pasto Ventura, and 0.1-0.2 wt.% in Campo Negro (Supplementary material, Table S7). The Ti concentrations in oxide mineral inclusions in phenocrysts also vary among the centers in the same order as shown by the groundmass phases. Thus, oxide inclusions in the Pasto Ventura samples have the highest Ti contents (21-34 wt.% TiO_2), those from Campo Negro have the lowest values (0.03-0.3 wt.%, TiO_2) and the Carachipampa oxide inclusions are intermediate. The olivine phenocrysts in Carachipampa andesite contain inclusions of Cr-rich spinel [Cr# [Cr/(Cr + Al)] = 0.6-0.7]. Risse et al. (2013) and Maro et al. (2017a) also reported spinel inclusions in phenocrysts of olivine-bearing mafic andesites in the Southern and Northern Puna, respectively.

Amphibole

Amphiboles from all Puna centers studied here belong to the calcic group of Leake et al. (1997) and mostly classify as magnesio-hastingsite. Pargasitic compositions are common in Campo Negro samples (both in the cores and the rims), but are found only in the rims of some amphibole crystals in Pasto Ventura. For simplicity, these phases will be referred to throughout the manuscript as amphiboles. Two compositional groups can be distinguished based on their Ti and Al contents (Fig. 6A). The more widespread of the two is here referred to as low Ti-Al (< 3 wt. % TiO_2 and < 13 wt. % Al_2O_3). The high Ti-Al amphiboles are also characterized by higher K (> 1 wt. % K_2O) and lower Na (< 2 wt. % Na_2O) than low Ti-Al amphiboles (< 1 wt. %, and > 2 wt. %, respectively). Both high- and low Ti-Al amphiboles have high Mg#, but the latter tends to be lower in the high Ti-Al group (71-74 versus 73-77 in the low Ti-Al group) (Table 3). All amphiboles analyzed, from both the high Ti-Al and low Ti-Al groups, have low Cl and F contents (typically 0.02-0.04 wt. % Cl and less than 0.1 wt. % F; see Table 3).

Regionally, amphibole phenocrysts in the Southern Puna centers (Carachipampa, Pasto Ventura) belong exclusively to the low Ti-Al group (Fig 6A). These are similar in composition to amphibole phenocrysts of andesites and dacites from the main arc of the Central Andes (Derruelle, 1991; Wittenbrink, 1997; Kraemer, 1999; Lindsay, 1999; Risse, 2008). The high Ti-Al amphiboles in this study are confined to the

Journal Pre-proof

Northern Puna Campo Negro center and resemble those present in the shoshonitic centers along the Calama-Olacapato-El Toro lineament (Derruelle, 1991; see Fig 6A). It is interesting that amphibole in the basaltic enclaves from Campo Negro are exclusively of the high Ti-Al group whereas the host lava contains both high Ti-Al amphiboles and some that are transitional between the two main groups (Fig. 6A).

In most cases, amphibole phenocrysts and microphenocrysts in a given sample have similar concentrations of Ca, Na, Fe, K, Mn, and Mg, with the exception of Ti that varies between lava and enclave crystals, as mentioned before. The Pasto Ventura samples also show some special features. In particular, the cores of the large skeletal phenocrysts in Pasto Ventura have higher Mg# than the microphenocrysts, whereas the rims are similar to the more frequent phenocrysts. These large crystals can be interpreted as antecrysts that formed prior to the other amphiboles, probably from a less-evolved, Mg-rich andesite or basaltic andesite magma ($Mg\#_{amp}$ >79; Moore and Carmichael, 1998; Grove et al. 2003). This type of amphibole, that is not equilibrated with the host rock, was not included in the thermobarometric analyses below. Most of the amphibole phenocrysts are internally homogeneous for the exception of the antecrysts in Pasto Ventura described above and a minor but inconsistent zoning in Si contents (ca. 2 wt.% difference in SiO_2), also in the Pasto Ventura samples (Table 3). Also, as mentioned above, opacite reaction rims are common throughout.

The trace element compositions among the low Ti-Al amphiboles (from Southern Puna centers) are similar in all samples studied, but they contrast with those of the high Ti-Al amphiboles from the Northern Puna in many ways. For example, the mantle-normalized multielement plot (Fig. 6B) reveals higher concentrations of most incompatible elements in the high Ti-Al amphiboles. This is especially true for the large ion lithophile elements (LILE), such as Rb and Ba which, like K as mentioned above, are notably enriched in the high Ti-Al group. Despite these differences in trace-element abundances, all groups show pronounced negative anomalies in Zr, Th and Rb, and less clearly in Nb and Ta. The bimodal distribution of amphibole compositions with respect to the Al and Ti contents is well displayed by the distribution of the Sr/Y values (Fig. 6C).

The chondrite-normalized REE diagram (Fig. 6D) shows convex-upward patterns that are typical for amphibole (Tiepolo et al., 2007; Nandedkar et al., 2016). Independent of the REE pattern, the total concentrations of REE in amphibole increase from Pasto Ventura to Carachipampa to the Campo Negro center. The distinction is stronger for the HREE than the LREE, which show parallel patterns whereas the patterns from MREE to HREE diverge. Negative Eu anomalies are commonly observed in calcic amphiboles, partly because the mineral-melt distribution coefficient for Eu (D_{Eu}) in amphibole is lower than the values for Sm and Gd (Green and Pearson, 1985; Tiepolo et al., 2007). However, the size of the Eu anomaly is not equal in all centers, being largest in the Campo Negro samples, which also show the largest negative Eu anomalies in bulk-rock compositions (Fig. 3B).

Concentrations of transition metals in amphibole (such as Ni) also show systematic differences between the low and high Ti-Al groups (see Supplementary material, Table S9). For example, Ni shows a good positive correlation with amphibole Mg#, hence Ni contents are lower in the high Ti-Al amphiboles in comparison with the low Ti-Al amphiboles from the Southern Puna centers (Table 4). Copper concentrations show variations between the high Ti-Al and low Ti-Al amphiboles (Fig. 7A). The amphibole in Campo Negro basaltic enclave is poor in this element (4 to 7 µg/g) and shows no variation from core to rim. Copper concentrations are generally higher in the low Ti-Al amphiboles in the Southern Puna mafic centers and also more variable. Some of this range may be related to unseen inclusions in the case of obvious outlier values, but we also note differences in core and rim concentrations, yet without systematic trends. The total range of values from Carachipampa phenocrysts is 13 to 502 µg/g but most values are between 200 and 400 µg/g. Concentrations are lower in Pasto Ventura (total range: 13 to 240 µg/g, mainly between

50 and 70 μg/g).

Like copper, lithium shows higher concentrations in the low Ti-Al amphiboles from the Southern Puna centers (ca. 100-200 μg/g) than in the high Ti-Al group (40-55 μg/g) (Table 3). The data from the Pasto Ventura and Carachipampa centers define well-developed trends between both elements (Fig. 7B) and these trends differ from one sample to another (see figure caption for regression lines a, b, c and d). Samples-specific correlation trends between Cu and Li in amphibole in arc andesites was also noted by Chiaradia et al. (2012) from a study of Pilavo volcano, Ecuador. Shallower slopes (lower Cu/Li) in that study were found in the more evolved rocks, which were suggested to reflect loss of Cu preferential to Li during magma degassing. The systematics of Li and Cu behavior in amphibole was discussed at length by Rowe et al. (2008) in a study of Mt. St. Helens dacite. The covariance of these elements across a wide compositional range was related to similarly high rates of diffusion in amphibole, allowing both elements to adjust to changing melt compositions during magma ascent and evolution.

DISCUSSION

Factors controlling the high- vs. low Ti-Al amphibole groups

In amphibole, like biotite and many other minerals, Ti contents commonly increase with temperature (Ernst and Liu, 1998), hence, temperature variations may partly explain variations in the Ti content of amphiboles. Nevertheless, a more likely factor, that affects both Ti and Al, is the melt composition. Molina et al. (2009) found that amphiboles crystallized from alkaline melts tend to have higher Ti and Al contents than those from subalkaline systems. Note that the Campo Negro (high Ti-Al) amphibole plots in the alkaline field in Figure 9A, B while Southern Puna amphiboles plot in the subalkaline field. In addition, the bulk compositions of Campo Negro lavas and basaltic enclave are significantly enriched in K_2O at a given SiO_2 content compared with the Southern Puna rocks (Fig. 2A). Maro et al. (2017a) found evidence for two distinct mantle components contributing to the primary magmas of the Puna mafic centers based on trends of Nd- and Sr initial isotope ratio with MgO. The data from Southern Puna centers showed trends consistent with an origin from the depleted mantle wedge. However, samples from the Campo Negro center (and other monogenetic volcanoes from Northern Puna) defined a separate trend that suggested an enriched mantle source that Maro et al. (2017a) attributed to lithospheric delamination. The production of hydrous magma with alkaline affinity in Campo Negro could thus be explained by mixing of primary melts produced from the lithospheric mantle (pyroxenite/eclogite) and from the asthenospheric peridotite (e.g., Straub el et. 2008).

The trace element compositions of a melt in equilibrium with amphibole were estimated with the multiple regression approach of Humphreys et al. (2019) (see Supplementary material, Table S11). The results indicate that the high Ti-Al amphiboles (Northern Puna) are in equilibrium with magmas richer in Nb. High Ba contents in the high Ti-Al amphiboles (> 250 ppm) also indicate enrichment in Ba in the related melts. High Ba and Nb are signatures observed in alkaline arc (Cruz Uribe et al., 2018) and shoshonitic back-arc lavas (Derruelle, 1991; Kay et al., 1994).

Another important difference in the predicted melt compositions from the high Ti-Al and low Ti-Al amphiboles is a contrast in the Sr/Y ratios (Fig. 9C). The low Ti-Al-derived melts (corresponding to Southern Puna) have higher Sr/Y values than the other group and the same contrast is observed for La/Yb ratios (Fig. 9D). Trace element compositions of the high Ti-Al amphibole from Campo Negro andesite are not available to calculate melt Sr/Y ratios, but the bulk-rock Sr/Y ratios in the andesitic rocks are lower than those from the Southern Puna centers (see Table 1). This is an important point because a high Sr/Y ratio is commonly considered to indicate relatively high-pressure crystallization and/or high water content of melts (not mutually exclusive), which can be favorable conditions for Cu enrichment in magmas (Richards, 2011; Chiaradia

Journal Pre-proof

et al., 2012). Several experimental studies (e.g., Sisson and Grove, 1993; Blatter and Carmichael, 1998; Blatter and Carmichael, 2001; Barclay and Carmichael, 2004) showed that dry basalts crystallized at deep- or shallow-conditions saturate with plagioclase early, while more than 3 wt.% of H_2O in the melt inhibits the crystallization of plagioclase as a phenocryst in magmas at crystallizing mid- to lower crustal pressures. Amphibole is stabilized in hydrous, high-pressure magmas and its crystallization causes depletions in Y and HREE (Macpherson et al., 2006; Alonso-Pérez et al., 2009; Richards, 2011). These two factors will contribute to high Sr/Y ratios. A suppression of plagioclase crystallization for the Southern Puna magmas is consistent with the lack of plagioclase phenocrysts and the relatively high Sr contents. On the other hand, plagioclase (with $An_{<90}$) is a phenocryst phase in the Northern Puna lava and enclaves, and there are geochemical signs of plagioclase fractionation in bulk rock, including lower Sr contents and well-developed Eu anomalies. This might suggest less hydrous parental melts and/or shallower magma evolution than in the Southern Puna centers (Sisson and Grove, 1993; Müntener et al., 2001).

Amphibole-melt equilibria and crystallization conditions

Maro et al. (2017a) calculated mineral-melt equilibrium P-T conditions for two samples from the Northern Puna (Campo Negro CN09-2 and CN09-5) containing orthopyroxene and plagioclase microphenocrysts. The orthopyroxene-melt results (Putirka, 2008) indicate 1238 to 1270°C and 0.7 to 8 kbar, plagioclase-melt temperature estimates were 1122 to 1158°C, consistent with the later appearance of that mineral in the crystallization sequence of crystallization. That study reported 1000°C and 5 kbar from amphibole-melt equilibria based on Ridolfi et al. (2010). In this paper we expand on the work of Maro et al. (2017a) by focusing on amphibole-melt equilibria, adding more data that is filtered for equilibrium compositions, and also comparing different calibrations. No previous work was done on amphibole crystallization conditions in the Southern Puna centers.

The application of mineral equilibria to calculate P-T conditions relies on the assumption that the amphiboles have equilibrium compositions with respect to the host rocks. Crystal rim compositions were rejected because of the common reaction textures (see Fig. 4). Core compositions were tested for equilibrium by comparing the host-rock SiO_2 content with the values predicted for a silicate melt in equilibrium with calcic amphibole (Ridolfi and Renzulli, 2012; Putirka, 2016). The observed and predicted values agreed within the mean error of ± 3.6 wt. % SiO_2 in several samples from Carachipampa (Tables 3 and 5). Deviations from equilibrium predict more silicic liquids (dacitic) than observed, a common result for amphibole in the Pasto Ventura samples. In the Northern Puna Campo Negro samples, amphibole compositions are commonly in equilibrium with the respective andesite lava or basalt enclave whole rock. However, there are also cases where the predicted melt SiO_2 for amphibole from andesite lava is lower by 5 to 10 wt. % than the host rock composition and close to that of the basaltic enclave, whereas the opposite is true for some amphiboles from the enclave. This suggests a probable interchange of amphibole crystals between the basaltic magma and the andesitic host during magma mingling. For the application of thermobarometry we consider as suitable only core compositions from amphibole crystals whose calculated melt SiO_2 differs by no more than the 3.6 wt.% from the SiO_2 content of the host rock.

Ridolfi et al. (2010) and Ridolfi and Renzulli (2012) provided equations for calculating intensive parameters of crystallization from amphibole composition, which are calibrated for a large compositional range from mafic to intermediate magmas of calc-alkaline to alkaline affinity, from H_2O-poor to H_2O-rich, and a wide range of pressures and temperatures, with moderately reduced to moderately oxidized conditions. The two formulations are in good agreement for our samples and yield similar crystallization temperatures among the centers (Table 5), and an apparent increase from Pasto Ventura (960-980 °C), to Carachipampa (985-1000 °C), to Campo Negro andesitic lava (995-1010 °C), to the Campo Negro basaltic enclave (1000-1020 °C), although we note that the differences are close to the estimated uncertainty of ± 22 °C (Ridolfi et al., 2010). Temperatures from the amphibole-melt thermometer of Putirka (2016) agree with those from the other thermometers (Fig. 8A).

Pressure calculations based on amphibole equilibria have been called into question by some authors (Bachmann and Dungan, 2002; Erdmann et al., 2014; Putirka, 2016) and there is a high error (± 4 kbar) in the barometers developed by Ridolfi et al. (2010) and Ridolfi and Renzulli (2012). This is attributed to the poor sensitivity of Al concentrations to pressure change (Putirka, 2016, Zhang et al., 2017), combined with the dependence of pressure on water concentrations in the melt (Putirka, 2016). Taking the latter into account, Putirka (2016) proposed new calibrations that reduce the error to ±1 kbar. Applied to the Puna amphibole data, the calibration of Putirka (2016, eq. 7a) yields pressures that correlate very well with those of Ridolfi and Renzulli (2012, eq.1a and 1b), but the latter yield systematically lower values by about 1 kbar (Fig. 8B). Both the numerical agreement and the correlation of the values are worse for the Ridolfi and Renzulli (2012) equations 1c and 1d (Fig. 8C, D), despite the recommendation of the latter by Ridolfi and Renzulli (2012, 2014) and Putirka (2016). The results suggest that high Ti-Al amphiboles from the Campo Negro center crystallized at higher pressure (8-6 kbar) than the low Ti-Al amphiboles at Pasto Ventura (4-3 kbar). The amphibole phenocrysts in the Carachipampa samples show considerable discrepancies among different barometers (Table 3), but all suggest relatively low crystallization pressures, similar to Pasto Ventura and in agreement with their low Al content.

Mineral-melt equilibrium geothermobarometry based on olivine, clinopyroxene and orthopyroxene (e.g., Putirka, 2008) was also applied to the studied samples, following the methods and considerations explained in Maro et al. (2017a) (Table S6). When P-T estimations require input of melt H_2O concentration, a minimum value of 3.5 wt.% was considered based on the stability of magnesio-hastingsite (Ridolfi et al., 2010). For both Northern and Southern Puna samples, clinopyroxene started to crystallize at 10 kbar and the temperature estimates indicates ~1150 to ~1170 °C, in concomitance with olivine formation (~ 1150 °C - 1200 °C, see Table 6). Plagioclase thermometry (Putirka, 2008) applied to the Campo Negro lava and its enclave yielded overlapping estimated maximum temperatures of 1020-1050 °C. The P-T estimates for olivine and pyroxene crystallization are higher than those estimated for amphibole, suggesting early crystallization of olivine and pyroxene assemblage before the magmas entered the amphibole stability field by cooling and rise in melt water contents (e.g., Sisson and Grove, 2003; Barclay and Carmichael, 2004). The temperature estimates from plagioclase-melt thermometry in Campo Negro are similar to those for amphibole from the same center, suggesting that both minerals crystallized together.

Although the results of fO_2 estimates following Ridolfi et al. (2010) and Ridolfi and Renzulli (2012) have significant uncertainties (Erdmann et al. 2014, Putirka 2016), they suggest relatively oxidized magma (1.2 to 1.4 log units above the NNO buffer for samples in the Southern Puna and less, ~0.5 log units above NNO, for Campo Negro lavas and basaltic enclave; Table 5). Finally, the water contents (following Ridolfi et al., 2010) of melts in equilibrium with amphibole were estimated at around 5 wt.%, with no significant difference between Southern and Northern Puna samples (Table 5).

Significance of partial melting zones in the crust

The compositional differences between the mafic centers in the Northern and Southern Puna in terms of amphibole may be related to their locations relative to zones of partial melting in the middle to upper crust inferred from geophysical anomalies, which differ greatly in size (Ward et al.. 2014) (Fig. 10). Thus, the Northern Puna Campo Negro center lies above the area of the Altiplano-Puna Magmatic Body (APMB, Fig. 10A), which is a first-order feature related to a regional-scale Neogene ignimbrite province (e.g., Chmielowski et al., 1999; Kay et al., 2010; de Silva and Kay, 2018). By contrast, the Southern Puna centers Pasto Ventura and Carachipampa lie south of the APMB and above the border of the Cerro Galán Magmatic Body (Fig. 10B). Whereas the extent of the partial melting zone in the Southern Puna has probably never been wider than it is now (Ward et al., 2014), the APMB is much larger and longer-lived (based on ignimbrite ages, Kay et al., 2010), and is set in a thermally more mature crust (Ward et al., 2014).

These contrasts in the structure of the crust below the mafic centers can affect the trajectories and duration of magma ascent to surface and, thus, their compositional evolution. We suggest that the smaller size and deeper location of the partial melting zone below the Southern Puna, and the location of the two centers at its margin (Fig. 10B), favored faster ascent of the hydrous magmas without significant stalling after leaving the deep crustal reservoir. The skeletal shape of amphibole phenocrysts in the Southern Puna centers supports this hypothesis. In contrast, the thicker and longer-lived Altiplano-Puna partial melting zone acted as a more efficient mechanical and/or rheological barrier for magma ascent in the Northern Puna. Those magmas therefore experienced considerable slowing of ascent in the mid-upper crust, which favored plagioclase saturation at lower pressure and/or due to water exsolution. Bulk-rock chemical and Sr-Nd isotope data reported by Maro et al. (2017a) support the idea that the APMB affected magma evolution in the Northern Puna centers more than those in the south.

Preliminary implications for Cu transport in Puna mafic magmas

From the few bulk-rock data available, the bulk-rock Cu concentrations in the Puna centers studied here appear to be similar although possibly lower in the Campo Negro center in the north (25 μg/g) than in Pasto Ventura and Carachipampa in the south (37 and 54 μg/g, respectively, Table 1). However, bulk-rock values can be misleading because of Cu loss prior to eruption, so Cu concentration in early-crystallized amphibole may be a better proxy for the magma concentrations, as suggested by Hsu et al. (2017).

Our LA-ICPMS analyses of amphibole phenocrysts reveal considerable within-grain variations in Cu contents (Supplementary material, Table S9). Because our interest is in constraining Cu concentrations in the parental melt, this discussion uses only data from grain cores and excludes any local extreme values that likely relate to sulfide inclusions. Compared in this way, the Northern Puna Campo Negro amphiboles are consistently much lower in Cu, with 4-7 μg/g (ave. 4.6±1.5), than those from the Southern Puna centers. Amphibole from Pasto Ventura yielded values of 23-73 μg/g (ave. 67±18, excluding two outliers with 234 and 240 μg/g), and the highest Cu values were found in Carachipampa amphiboles, with 206-309 μg/g (ave. 260±41, excluding one outlier at 73 μg/g). Considering that D_{Cu} (amph/melt) values are considerably less than one (Lee et al., 2012; Liu et al., 2015; Hsu et al., 2017), the results imply high melt concentrations of Cu in the Southern Puna at the time of amphibole crystallization and correspondingly lower concentrations in the magmas beneath the Northern Puna centers when amphibole crystallization occurred.

The low Cu concentration in Northern vs. Southern Puna mafic magmas inferred from the amphibole data could be interpreted as a feature of the primitive magmas in the two regions. However, the behavior of Cu in mafic magmas is complex and how amphibole Cu contents are affected depends on the relative timing of crystallization vs. Cu loss (or gain) and on the balance between Cu diffusion rates in amphibole and the ascent rates of the hosting magma magmas and/or longer residence time at depth (e.g., Chiaradia et al., 2012). More research in the Cu budget of these rocks including other mineral phases and their inclusions is needed to resolve this. It would also be useful to study the ultramafic xenoliths (mostly pyroxenites) that are known to exist in basaltic andesites in the Northern Puna region (Maro et al., 2016) because they may be cumulate residues derived from differentiation of primitive basaltic magmas at the base of the crust, as has long been postulated for the Central Andes arc (Hildreth and Moorbath, 1988). These xenoliths would be relevant to assess the hypothesis of early Cu loss by sulphide sequestration in the lower/middle crust (Lee et al., 2012; Chiaradia, 2014; Jenner et al., 2017; Hou and Wang, 2019).

On the other hand, the Cu concentrations estimated for mafic magmas beneath the Southern Puna centers are well above the typical values for CVZ arc magmas and higher than the corresponding bulk-rock values. We may postulate that the primitive magmas in this region were unusually Cu-rich, possibly from remelting sulphide-bearing lower crust in the course of delamination postulated for this region (e.g., Kay and Kay, 1993). Still, significant loss of Cu occurred after amphibole crystallization and the amphibole crystals did not readjust to the changing melt composition, possibly because of the relatively fast ascent (skeletal crystal forms). Detailed study is needed on the Cu budget in these rocks and their mineral phases to confirm and explain the apparent Cu enrichment in the Southern Puna primitive magmas, what prevented loss of Cu in the magmas prior to amphibole crystallization and what were the causes of Cu loss before eruptions.

SUMMARY AND CONCLUSIONS

Amphibole-bearing mafic andesites from the Neogene volcanism in the Puna plateau of the Central Andes indicate the presence of hydrous parental magmas in this region. This study focuses on the petrology and geochemistry of amphibole phenocrysts, associated minerals and host-rock composition from high-Mg andesitic lavas and a basaltic enclave from the Southern and Northern segments of the Puna. Two contrasting amphibole phenocryst types were found, a high Ti and Al group that is found in the Northern Puna basaltic enclave and host high Mg andesitic lava, and a low Ti and Al group, which occurs in all Southern Puna samples. Thermobarometric analyses imply crystallization in deep and hot reservoirs (1000-1020 °C and 8-6 kbar) for the high Ti-Al type and middle to low pressures and somewhat lower temperatures (< 1000 °C and < 5 kbar) of formation for the low Ti-Al type. An olivine and clinopyroxene assemblage in the Southern Puna or orthopyroxene in the Northern Puna crystallized before amphibole, in both cases at around 10 kbar and at ~ 1200 °C.

Chemical features of the Southern Puna lavas and of parental melts calculated from the amphibole trace-element partitioning suggest plagioclase-free, high pressure differentiation of hydrous magmas (high Sr/Y and La/Yb ratios, lack of Eu anomaly) whereas in the Northern Puna, lower Sr/Y ratios, a well-developed negative Eu anomaly in REE diagrams and the presence of plagioclase phenocrysts imply magma evolution at shallower levels in the crust. These differences can be related to the presence of a large, ca. 11 km-thick partial melting zone (APMB) inferred from geophysics below the Northern Puna, which is less well-developed and deeper in the south. The APMB may have caused slower ascent and more interaction with felsic magmas and/or crustal assimilation in the Northern Puna magmas than in the south (see also Maro et al., 2017a). In addition, the high Ti and Al contents in amphibole phenocrysts in the high Mg andesites from the Northern Puna imply the participation of alkaline melts in this region.

There are large differences in the Cu contents of amphibole from the Southern and Northern Puna. Copper contents are uniformly low (4-7 μg/g) in the Northern Campo Negro center, while the amphibole from Pasto Ventura and Carachipampa in the south yielded wider ranges and higher values, typically 50-73 μg/g, and about 200-400 μg/g, respectively. These values give first evidence of a major difference between Cu in the respective magmas, with unusually high concentrations during amphibole crystallization and substantial loss of Cu before eruption beneath the Southern Puna.

AKNOWLEDGMENTS

The authors want to thank Ing. Patrocinio Flores (IdGyM-UNJu) and Paulino Cachizumba (IdGyM-UNJu) for preparation of bulk-rock chemical analyses, as well as Oona Appelt (GFZ Potsdam) for her assistance with microprobe analyses. The authors are also grateful for sharing samples and information about the Southern Puna monogenetic samples to Dr. Walter Báez (IBIGEO, CONICET-UNsa) and to Silvia Rosas (INECOA, CONICET-UNJu) for editorial support. A special thanks to Federico Ibarra (IGEBA, CONICET-UBA) for his contribution with the maps of the Bouguer anomalies for the Puna. The authors thank Massimo Chiaradia and Martin Streck for the very helpful reviews that significantly improved the text.

Journal Pre-proof

This research was funded by the CONICET-DFG GII Cooperation Project A.4.2 “Transport of metals by shallow-level felsic magmas in the Cu-Au and Sn-Ag ore belts in the southern central Andes” within the framework of the International Research Training Group IGK2018 “SuRfAce processes, TEctonics and Georesources: The Andean foreland basin of Argentina” (StRATEGy)”, by the Agencia Nacional de Promoción Científica y Técnica (PICT 2016-N°0044), and by SECTER-UNJu (E-B004).

REFERENCES

Allmendinger, R. W., Jordan, T. E., Kay, S.M., Isacks, B.L., 1997. The evolution of the Altiplano-Puna plateau of the Central Andes. Annual Review of Earth and Planetary Sciences, 25, 139-174.

Alonso, R.N., Viramonte, J.G., 1987. Geología y metalogenia de la Puna. Estudios Geológicos, 43, 393-407.

Alonso-Pérez, R., Müntener, O., Ulmer, P., 2009. Igneous garnet and amphibole fractionation in the roots of island arcs: experimental constraints on andesitic liquids. Contributions to Mineralogy and Petrology, 157, 541-558.

Applegarth, L.J., Tuffen, H., James, M.R., Pinkerton, H., Cashman, K.V., 2013. Direct observations of degassing-induced crystallization in basalts. Geology, 41 (2), 243-246.

Aquater, A., 1979. Estudio del potencial geotermico de la Provincia de Jujuy, República Argentina. Secretaria de Estado de Minería, Contrato Saipen Argentina S.A., Gobierno de Jujuy, 1-129.

Bachmann, O., Dungan, M.A., 2002. Temperature-induced Aluminium zoning in hornblendes of the Fish Canyon magma, Colorado. American Mineralogist, 87, 1062-1076.

Báez, W., Carrasco-Núñez, G., Giordano, G., Viramonte, J., Chiodi, A., 2017. Polycyclic scoria cones of the Antofagasta de la Sierra basin,

Journal Pre-proof

Southern Puna plateau, Argentina, in: Németh, K., Carrasco Núñez, G., Aranda-Gómez, J., Smith, I. (Eds.), Monogenetic volcanism. The Geological Society of London, Special Publications, 446, 311-336.

Barclay, J., Carmichael, I.S.E., 2004. A hornblende basalt from western Mexico: water-saturated phase relations constrain a pressure-temperature window of eruptibility. Journal of Petrology, 45, 485-506.

Beck, S.L., Zandt, G., Ward, K.M., Scire, A., 2015. Multiple styles and scales of lithospheric foundering beneath the Puna Plateau, Central Andes, in: DeCelles, P.G., Ducea, M.N., Carrapa, B., and Kapp, P.A. (Eds.), Geodynamics of a Cordilleran Orogenic System: The Central Andes of Argentina and Northern Chile. Geological Society of America Memoirs, 212, 43-60.

Stremel, B.R., 2016. O Sistema Magmático do Depósito de Cu-Mo Tipo Pórfiro Pancho Árias, Cordilheira Oriental, Argentina. MSc Thesis. Universidade de Brasília. Instituto de Geociências. Programa de pos graduação em Geologia. 94 p.

Bianchi, M., Heit, B., Jakovlev, A., Yuan, X., Kay, S.M., Sandvol, E., Comte, D., 2013. Teleseismic tomography of the southern Puna plateau in Argentina and adjacent regions. Tectonophysics, 586, 65-83.

Blatter, D.L., Carmichael, I.S.E., 1998. Plagioclase-free andesites from Zitacuaro (Michoacán), Mexico: petrology and experimental constraints. Contributions to Mineralogy and Petrology, 132, 121-138.

Blatter, D.L., Carmichael, I.S.E., 2001. Hydrous phase equilibria of a Mexican siliceous andesite: a candidate for a mantle origin? Geochimica et Cosmochimica Acta, 65 (21), 4043-4065.

Blundy, J., Cashman, K., 2001. Ascent-driven crystallisation of dacite magmas at Mount St Helens, 1980-1986. Contributions to Mineralogy and Petrology, 140, 631-650.

Browne, B.L., Gardner, J.E., 2006. The influence of magma ascent path on the texture, mineralogy and formation of hornblende reaction rims. Earth and Planetary Science Letters, 246, 161-176.

Caffe, P.J., Trumbull, R.B., Coira, B.L., Romer, R.L., 2002. Petrogenesis of Early Neogene magmatism in the Northern Puna; implications for magma genesis and crustal processes in the Central Andean Plateau. Journal of Petrology, 43, 907-942.

Carmichael, I.S.E., 2002. The andesite aqueduct: perspectives on the evolution of intermediate magmatism in west-central (105-99ºW) Mexico. Contributions to Mineralogy and Petrology, 143, 641-663.

Chernicoff, C. J., Richards, J. P., Zappettini, E. O., 2002. Crustal lineament control on magmatism and mineralization in northwestern Argentina: geological, geophysical, and remote sensing evidence. Ore Geology Reviews, 21(3-4), 127-155. Chiaradia, M., Ulianov, A., Kouzmanov, K., Beate, B., 2012. Why large porphyry Cu deposits like high Sr/Y magmas? Nature Scientific Reports, 2, 685.

Chiaradia, M., 2014. Copper enrichment in arc magmas controlled by overriding plate thickness. Nature Geoscience, 7(1), 43-46.

Chiaradia, M., Caricchi, L., 2017. Stochastic modelling of deep magmatic controls on porphyry copper deposit endowment. Scientific reports, 7(1), 1-11.

Chmielowski, J., Zandt, G., Haberland, C., 1999. The central Andean Altiplano-Puna magma body. Geophysical Research Letters, 26, 783-786.

Coira, B., Kay, S.M., Viramonte, J.G., 1993. Upper Cenozoic magmatic evolution of the Argentine Puna-A model for changing subduction geometry. International Geology Review, 35, 677-720.

Corneau, M.J., Unsworth, M.J., Cordell, D., 2016. New constraints on the magma distribution and composition beneath Volcán Uturuncu and the southern Bolivian Altiplano from magnetotelluric data. Geosphere, 12 (5), 1-31.

Journal Pre-proof

Cruz-Uribe, A.M., Marschall, H.R., Gaetani, G.A., Le Roux, V., 2018. Generation of alkaline magmas in subduction zones by partial melting of mélange diapirs—An experimental study. Geology, 46(4), 343-346.

Dalpé, C., Baker, D.R., 2000. Experimental investigation of large-ion lithophile-element-high-field-strength element- and rare-earth-element-partitioning between calcic amphibole and basaltic melt: the effects of pressure and oxygen fugacity. Contribution to Mineralogy and Petrology, 140, 233-250.

De Angelis, S.H., Larsen, J., Coombs, M., 2013. Pre-eruptive magmatic conditions at Augustine Volcano, Alaska, 2006: evidence from amphibole geochemistry and textures. Journal of Petrology, 54, 1939-1961.

De Angelis, S.H., Larsen, J., Coombs, M., Dunn, A., Hayden, L., 2015. Amphibole reaction rims as a record of pre-eruptive magmatic heating: An experimental approach. Earth and Planetary Science Letters, 426, 235-245.

Deruelle, B., 1991. Petrology of Quaternary shoshonitic lavas of northwestern Argentina. In: Harmon, R.S. and Rapela, C.W., eds, Andean Magmatism and its Tectonic Setting. Geological Society of America Special Paper 265, 201-216.

de Silva, S.L., 1989. The Altiplano-Puna volcanic complex of the central Andes. Geology, 17, 1102-1106.

de Silva, S. L., Kay, S. M., 2018. Turning up the heat: High-flux magmatism in the Central Andes. Elements, 14(4), 245-250.

Defant, M.J., Drummond, M.S., 1990. Derivation of some modern arc magmas by melting of young subducted lithosphere. Nature, 347, 662-665.

Ducea, M.N., Seclaman, A.C., Murray, K.E., Jianu, D., Schoenbohm, L.M., 2013. Mantle-drip magmatism beneath the Altiplano-Puna plateau, Central Andes. Geology, 41, 915-918.

Erdmann, S., Martel, C., Pichavant, M., Roma, A., Kushnir, L., 2014. Amphibole as an archivist of magmatic crystallization conditions: problems, potential, and implications for inferring magma storage prior to the paroxysmal 2010 eruption of Mount Merapi, Indonesia. Contributions to Mineralogy and Petrology, 167, 1-23.

Ernst, W. G., Liu, J., 1998. Experimental phase-equilibrium study of Al-and Ti-contents of calcic amphibole in MORB—A semiquantitative thermobarometer. American mineralogist, 83(9-10), 952-969.

Filipovich, R., Báez, W., Bustos, E., Villagrán, A., Chiodi, A., Viramonte, J.G., 2019. Estilos eruptivos asociados al volcanismo monogenético máfico de la región de Pasto Ventura, Puna Austral, Argentina. Andean Geology, 46 (2), 300-335.

Fricker, M.B., 2012. Design of ablation cells for LA-ICP-MS, ETH Zürich. doi:10.3929/ethz-a- 007615617.

Green, T.H., Pearson, N.J., 1985. Experimental determination of REE partition coefficients between amphibole and basaltic to andesitic liquids at high pressure. Geochimica et Cosmochimica Acta, 49, 1465-1468. doi: 10.1016/0016-7037(85)90295-9.

Grove, T.L., Elkins-Tanton, L.T., Parman, S.W., Chatterjee, N., Muntener, O., Gaetani, G.A., 2003. Fractional crystallization and mantle-melting controls on calc-alkaline differentiation trends. Contributions to Mineralogy and Petrology, 145, 515-533.

Guzmán, S.R., Petrinovic, I.A., Brod, J.A., 2006. Pleistocene mafic volcanoes in the Puna-Cordillera Oriental boundary, NW-Argentina. Journal of Volcanology and Geothermal Research, 158, 51-69.

Haberland, C., Rietbrock, A., Schurr, B., Brasse, H., 2003. Coincident anomalies of seismic attenuation and electrical resistivity beneath the southern Bolivian Altiplano plateau. Geophysical Research Letters, 30, 1-4.

Halter, W. E., Bain, N., Becker, K., Heinrich, C. A., Landtwing, M., VonQuadt, A., Clark, A.H., Sasso, A.M., Bissig, T. , Tosdal, R. M., 2004. From andesitic volcanism to the formation of a porphyry Cu-Au mineralizing magma chamber: the Farallón Negro Volcanic Complex, northwestern Argentina. Journal of Volcanology and Geothermal Research, 136(1-2), 1-30.

Halter, W. E., Heinrich, C. A., Pettke, T., 2005. Magma evolution and the formation of porphyry Cu–Au ore fluids: evidence from silicate and sulfide melt inclusions. Mineralium Deposita, 39(8), 845-863.

Hattori, K. H., Keith, J. D. 200). Contribution of mafic melt to porphyry copper mineralization: evidence from Mount Pinatubo, Philippines, and Bingham Canyon, Utah, USA. Mineralium Deposita, 36(8), 799-806.

Hawthorne, F.C., 1981. Crystal chemistry of the amphiboles, in: Veblen D.R. (Ed.), Amphiboles and other hydrous pyriboles-mineralogy. Mineralogical Society of America Reviews in Mineralogy and Geochemistry, 9A, 1-102.

Heit, B., Koulakov, I., Asch, G., Yuan, X., Kind, R., Alcocer-Rodriguez, I., Wilke, H., 2008. More constraints to determine the seismic structure beneath the Central Andes at 21°S using teleseismic tomography analysis. Journal of South American Earth Sciences, 25, 22-36.

Hildreth, W., Moorbath, S., 1988. Crustal contributions to arc magmatism in the Andes of central Chile. Contributions to Mineralogy and Petrology, 98(4), 455-489.

Holland, T., Blundy, J., 1994. Nonideal interactions in calcic amphiboles and their bearing on amphibole-plagioclase thermometry. Contributions to Mineralogy and Petrology, 116, 433-447.

Hou, Z., Wang, R. 2019. Fingerprinting metal transfer from mantle. Nature communications, 10(1), 1-3.

Hsu, Y. J., Zajacz, Z., Ulmer, P., Heinrich, C. A., 2017. Copper partitioning between silicate melts and amphibole: Experimental insight into magma evolution leading to porphyry copper ore formation. Chemical Geology, 448, 151-163.

Humphreys, M. C., Cooper, G. F., Zhang, J., Loewen, M., Kent, A. J., Macpherson, C. G., Davidson, J. P., 2019. Unravelling the complexity of magma plumbing at Mount St. Helens: a new trace element partitioning scheme for amphibole. Contributions to Mineralogy and Petrology, 174(1), 9.

Jenner, F. E., 2017. Cumulate causes for the low contents of sulfide-loving elements in the continental crust. Nature Geoscience, 10(7), 524-529.

Jochum, K. P., Weis, U., Stoll, B., Kuzmin, D., Yang, Q., Raczek, I., Dorrit, E.J., Stracke, A., Birbaum, K., Frick., D.A., Günther, D., Enzweiler, J., 2011. Determination of reference values for NIST SRM 610–617 glasses following ISO guidelines. Geostandards and Geoanalytical Research, 35(4), 397-429.

Johnson, E.R., Wallace, P.J., Cashman, K.V., Delgado-Granados, H., Kent, A.J.R., 2008. Magmatic volatile contents and degassing-induced crystallization at Volcán Jorullo, Mexico: Implications for melt evolution and the plumbing systems of monogenetic volcanoes. Earth and Planetary Science Letters, 269, 477-486.

Kay, R.W., Kay, S.M., 1993. Delamination and delamination magmatism. Tectonophysics, 219, 177-189.

Kay, S. M., Mpodozis, C., 2001. Central Andean ore deposits linked to evolving shallow subduction systems and thickening crust. Geological Society of America Today, 11, 4-9

Kay, S.M., Coira, B., Viramonte, J., 1994. Young mafic back arc volcanic rocks as indicators of continental lithospheric delamination beneath the Argentine Puna plateau, Central Andes. Journal of Geophysical Research, 99, 24323-24339.

Kay, S.M., Mpodozis, C., Coira, B., 1999. Magmatism, tectonism, and mineral deposits of the Central Andes (22°-33°S latitude). Geology and Ore Deposits of the Central Andes. Society of Economic Geology Special Publication, 7, 27-59.

Kay, S.M., Coira, B., Caffe, P.J., Chen, C-H., 2010. Regional chemical diversity, crustal and mantle sources and evolution of Central Andean

Journal Pre-proof

Puna Plateau Ignimbrites. Journal of Volcanology and Geothermal Research, 198, 81-111.

Kessel, R., Schmidt, M. W., Ulmer, P., Pettke, T. 2005. Trace element signature of subduction-zone fluids, melts and supercritical liquids at 120–180 km depth. Nature, 437(7059), 724.

Kraemer, B. 1999 Eine geochemische Traverse quer zum mittelmiozänen magmatischen Bogen im südlichen Bereich der Zentralen Vulkanischen Zone der Anden (ZVZ, 25° - 26°30´S, 67°30`- 69° W). PhD Thesis Freie Universitaet Berlin. Berliner Geowissenschaftliche Abhandlungen, A 200, 174 S.

Lee, C. T. A., Luffi, P., Chin, E. J., Bouchet, R., Dasgupta, R., Morton, D. M., Le Roux, V., Yin, Q., Jin, D., 2012. Copper systematics in arc magmas and implications for crust-mantle differentiation. Science, 336(6077), 64-68.

Lee, C. T. A., Tang, M., 2020. How to make porphyry copper deposits. Earth and Planetary Science Letters, 529, 115868.

Le Maitre, R.W., Bateman, P., Dudek, A., Keller, J., Lameyre, J., Le Bas, M.J., Sabine, P.A., Schmid, R., Sorensen, H., Strekeisen, A., Woolley, A.R., Zanettin, B., 1989. A classification of igneous rocks and glossary of terms: Recommendations of the International Union of Geological Sciences, Subcommission on the Systematics of Igneous Rocks (No. 552.3 CLA). International Union of Geological Sciences, 193 pp.

Li, J. X., Qin, K. Z., Li, G. M., Evans, N. J., Zhao, J. X., Yue, Y. H., Xie, J., 2018. Volatile variations in magmas related to porphyry Cu-Au deposits: Insights from amphibole geochemistry, Duolong district, central Tibet. Ore Geology Reviews, 95, 649-662.

Lindsay, J.M., 1999. Stratigraphy, age relations and magmatic evolution of large-volume felsic ignimbrites of the La Pacana Caldera, Central Andes, Chile. Scientific Technical Report STR99/16. GeoForschungsZentrum Potsdam, Potsdam, 141 pp.

Journal Pre-proof

Liu, Y., Hu, Z., Gao, S., Günther, D., Xu, J., Gao, C., Chen, H., 2008. In situ analysis of major and trace elements of anhydrous minerals by LA-ICP-MS without applying an internal standard. Chemical Geology, 257, 34-43.

Longerich, H.P., Jackson, S.E., Günther, D., 1996. Laser ablation inductively coupled plasma mass spectrometric transient signal data acquisition and analyte concentration calculation. Journal of Analytical Atomic Spectrometry, 11, 899-904.

Macpherson, C.G., Dreher, S.T., Thirlwall, M.F., 2006. Adakites without slab melting: high pressure differentiation of island arc magma, Mindanao, the Philippines. Earth and Planetary Science Letters, 243, 581-593.

Mamani, M., Wörner, G., Sempere, T., 2009. Geochemical variations in igneous rocks of the Central Andean orocline (13S to 18S): Tracing crustal thickening and magma generation through time and space. Geological Society of America Bulletin 122(1): 162-182.

Maro, G., Caffe, P.J., 2016. The Cerro Bitiche Andesitic Field: petrological diversity and implications for magmatic evolution of mafic volcanic centers from the northern Puna. Bulletin of Volcanology 78, 1-18.

Maro, G., Caffe, P.J., Jofré, C. 2016. Xenolitos ultramáficos en lavas máficas Neógenas de la Puna Norte. Revista de la Asociación Geológica Argentina 73, 280–291.

Maro, G., Caffe, P.J., 2017. Neogene monogenetic volcanism from the Northern Puna region: products and eruptive styles, in: Németh, K., Carrasco-Núñez, G., Aranda-Gómez, J.J., Smith, I.E. M. (Eds.), Monogenetic Volcanism. Geological Society of London, Special Publications, 446, 337-359.

Maro, G., Caffe, P. J., Romer, R. L., Trumbull, R. B. 2017a. Neogene mafic magmatism in the northern Puna Plateau, Argentina: generation and evolution of a back-arc volcanic suite. Journal of Petrology, 58(8), 1591-1617.

Journal Pre-proof

Maro, G., Caffe, P., Báez, W., 2017b. Volcanismo monogenético máfico cenozoico de la Puna, in: Muruaga C., Grosse P. (Eds.), Ciencias de la Tierra y Recursos Naturales del NOA. Relatorio del XX Congreso Geológico Argentino, 548-577.

Mazzuoli, R., Vezzoli, L., Omarini, R., Acocella, V., Gioncada, A., Matteini, M., Dini, A., Guillou, H., Hauser, N., Uttini, A., Scaillet, S. 2008. Miocene magmatism and tectonics of the easternmost sector of the Calama–Olacapato–El Toro fault system in Central Andes at~ 24 S: Insights into the evolution of the Eastern Cordillera. Geological Society of America Bulletin, 120(11-12), 1493-1517.

McGlashan, N., Brown, L.D., Kay, S.M., 2008. Crustal thicknesses in the Central Andes from teleseismically recorded depth phase precursors. Geophysical Journal International, 175, 1013-1022.

Molina, J. F., Scarrow, J. H., Montero, P. G., Bea, F. 2009. High Ti-Al amphibole as a petrogenetic indicator of magma chemistry: evidence for mildly alkalic-hybrid melts during evolution of Variscan basic-ultrabasic magmatism of Central Iberia. Contributions to Mineralogy and Petrology, 158(1), 69-98.

Moore, G., Carmichael, S.E., 1998. The hydrous phase equilibria (to 3 kbar) of an andesite and basaltic andesite from western Mexico: constraints on water content and conditions of phenocryst growth. Contributions to Mineralogy and Petrology, 130 (3-4), 304–319.

Müntener, O., Kelemen, P.B., Grove, T.L., 2001. The role of H_2O during crystallization of primitive arc magmas under uppermost mantle conditions and genesis of igneous pyroxenites: an experimental study. Contribution to Mineralogy and Petrology, 141, 643-658.

Murray, K.E., Ducea, M.N., Schoenbohm, L., 2015. Foundering-driven lithospheric melting: The source of central Andean mafic lavas on the Puna Plateau (22°S-27°S), in: DeCelles, P. G., Ducea, M.N., Carrapa, B., et al. (Eds.), Geodynamics of a Cordilleran Orogenic System: The Central Andes of Argentina and Northern Chile. Geological Society of America Memoir, 212, 139-166.

Journal Pre-proof

Nandedkar, R.H., Hurlimann, N., Ulmer, P., Müntener, O., 2016. Amphibole-melt trace element partitioning of fractionating calc-alkaline magmas in the lower crust: an experimental study. Contributions to Mineralogy and Petrology, 171 (8-9). doi: 10.1007/s00410-016-1278-0.

Peccerillo, A., Taylor, S.R., 1976. Geochemistry of Eocene calc-alkaline volcanic rocks from the Kastamonu area, northern Turkey. Contributions to mineralogy and petrology, 58(1), 63-81.

Pouchou, J.L., Pichoir, E., 1987. "PAP" (phirhoz) procedure for improved quantitative microanalysis. En: Armstrong, J.T. (Ed.), Microbeam Analysis, San Francisco Press, 104-106.

Presta, J.F., Caffe, P.J., 2014. Historia eruptiva de los volcanes monogenéticos de El Toro (23°05'S-66°42'O), Puna norte, Argentina. Andean Geology, 41, 142-173.

Prezzi, C.B., Götze, H.J., Schmidt, S., 2009. 3D density model of the Central Andes. Physics of the Earth and Planetary Interiors, 177, 217-234.

Putirka, K. 2016. Amphibole thermometers and barometers for igneous systems and some implications for eruption mechanisms of felsic magmas at arc volcanoes. American Mineralogist, 101 (4), 841-858.

Redford, S.D., Rice, S.M., 1997. Petrogenesis of Miocene basic shoshonitic lavas in the Bolivian Andes and implications for hydrothermal gold, silver and tin deposits. Journal of South American Earth Sciences, 10, 203-221.

Richards, J. P., 2011. High Sr/Y arc magmas and porphyry Cu±Mo±Au deposits: just add water. Economic Geology, 106(7), 1075-1081.

Ridolfi, F., Renzulli, A., 2012. Calcic amphiboles in calc-alkaline and alkaline magmas: thermobarometric and chemometric empirical equations valid up to 1,130°C and 2.2 GPa. Contributions to Mineralogy and Petrology, 163, 877-895.

Ridolfi, F., Renzulli, A., Puerini, M., 2010. Stability and chemical equilibrium of amphibole in calc-alkaline magmas: an overview, new thermobarometric formulations and application to subduction-related volcanoes. Contributions to Mineralogy and Petrology, 160, 45-66.

Risse, A., 2008. Goechronologie, Petrologie und Charakterisierung von Primärschmelzen mafischer Vulkanite des Puna-Plateaus der Zentralen Anden (NW - Argentinien. Doctoral Tesis Universität Potsdam, Mathematisch-Naturwissenschaftliche Fakultät / Institut für Geowissenschaften, 156 pp.

Risse, A., Trumbull, R.B., Coira, B., Kay, S.M., Van den Bogaard, P., 2008. $^{40}Ar/^{39}Ar$ geochronology of mafic volcanism in the back-arc region of the southern Puna plateau, Argentina. Journal of South American Earth Sciences, 26, 1-15.

Risse, A., Trumbull, R.B., Kay, S.M., Coira, B., Romer, R. L., 2013. Multi-stage evolution of late Neogene mantle-derived magmas from the central Andes back-arc in the Southern Puna Plateau of Argentina. Journal of Petrology, 54, 1963-1995.

Roeder P.L., Emslie, R., 1970. Olivine-liquid equilibrium. Contributions to Mineralogy and Petrology, 29, 275-289.

Rowe, M.C., Kent, A.J.R., Thornber, C.R., 2008. Using amphibole phenocrysts to track vapor transfer during magma crystallization and transport: an example from Mount St. Helens, Washington. Journal of Volcanology and Geothermal Research, 178, 593-607.

Rutherford, M.J., Devine, J.D., 2003. Magmatic conditions and magma ascent as indicated by Hornblende phase equilibria and reactions in the 1995-2002 soufriere hills magma. Journal of Petrology, 44 (8), 1433-1454.

Rutherford, M.J., Devine, J.D., 2008. The May 18, 1980, eruption of Mount St. Helens, 3, Stability and chemistry of amphibole in the magma chamber. Journal of Geophysical Research, 93, 11949-11959.

Rutherford, M.J., Hill, P.M., 1993. Magma ascent rates from amphibole breakdown: An experimental study applied to the 1980-1986 Mount St. Helens eruptions. Journal of Geophysical Research, 98, 19667-19685.

Salisbury, M.J., Jicha, B.R., de Silva, S.L., Singer, B.S., Jiménez, N.C., Ort, M.H., 2010. $^{40}Ar/^{39}Ar$ chronostratigraphy of Altiplano-Puna volcanic complex ignimbrites reveals the development of a major magmatic province. Geological Society of America Bulletin, B30280-1.

Schilling, F.R., Trumbull, R.B., Brasse, H., Haberland, C., Asch, G., Bruhn, D., Ramelow, J., 2006. Partial melting in the Central Andean crust: a review of geophysical, petrophysical, and petrologic evidence. In: Onken, O., Chong, G., Franz, G., et al. (Eds.), The Andes. Berlin: Springer, 459-474.

Schuessler, J.A., von Blanckenburg, F., 2014. Testing the limits of micro-scale analyses of Si stable isotopes by femtosecond laser ablation multicollector inductively coupled plasma mass spectrometry with application to rock weathering. Spectrochimica Acta, Part B: Atomic Spectroscopy, 98, 1-18.

Schurr, B., Rietbrock, A., Asch, G., Kind, R., Oncken, O., 2006. Evidence for lithospheric detachment in the central Andes from local earthquake tomography. Tectonophysics, 415, 203-223.

Seggiaro, R.E., 1994. Petrología, geoquímica y mecanismos de erupción del complejo volcánico Coranzulí. Tesis Doctoral (Inédita), Universidad Nacional de Salta, 1-230.

Sillitoe, R.H., 1977. Metallic mineralization affi liated to subaerial volcanism: a review, en Volcanic processes in ore genesis. Institution of Mining and Metallurgy, Geological Society of London, 99-116.

Sillitoe, R. H., 2010. Porphyry copper systems. Economic geology, 105(1), 3-41.

Sisson, T.W., Grove, T.L., 1993. Temperatures and H_2O contents of low-MgO high-alumina basalts. Contributions to Mineralogy and Petrology,

Journal Pre-proof

Journal Pre-proof

113, 167-184.

Sisson, T.W., Grove, T.L., 2003. Experimental investigations of the role of H_2O in calc-alkaline differentiation and subduction zone magmatism. Contributions to Mineralogy and Petrology, 113 (2), 143-166. doi: 10.1007/BF00283225.

Sobolev, A.V., Hofmann, A.W., Sobolev, S.V., Nikogosian, I.K., 2005. An olivine-free mantle source of Hawaiian shield basalts. Nature, 434(7033), 590.

Straub, S.M., LaGatta, A.B., Martin-Del Pozzo, A.L., Langmuir, C.H., 2008. Evidence from high-Ni olivines for a hybridized peridotite/pyroxenite source for orogenic andesites from the central Mexican Volcanic Belt. Geochemistry, Geophysics, Geosystems, 9(3).

Sun, S.S., McDonough, W.S., 1989. Chemical and isotopic systematics of oceanic basalts: implications for mantle composition and processes. Geological Society, London, Special Publications, 42(1), 313-345.

Sun, J.F., Yang, J.H., Wu, F.Y., Wilde, S.A., 2012. Precambrian crustal evolution of the eastern North China Craton as revealed by U-Pb ages and Hf isotopes of detrital zircons from the Proterozoic Jinggeryu Formation. Precambrian Research, 200-203, 184-208.

Tiepolo, M., Oberti, R., Zanetti, A., Vannucci, R., Foley, S.F., 2007. Trace-element partitioning between amphibole and silicate melt. Amphiboles: Crystal Chemistry, Occurrence, and Health Issues, 67, 417-451.

Wan, B., Deng, C., Najafi, A., Hezareh, M.R., Talebian, M., Dong, L., Dong, L., Chen, L., Xiao, W., 2018. Fertilizing porphyry Cu deposits through deep crustal hot zone melting. Gondwana Research, 60, 179-185.

Ward, K.M., Zandt, G., Beck, S.L., Christensen, D.H., McFarlin, H., 2014. Seismic imaging of the magmatic underpinnings beneath the Altiplano-Puna volcanic complex from the joint inversion of surface wave dispersion and receiver functions. Earth and Planetary Science Letters, 404, 43-53.

Wilkinson, J.J., 2013. Triggers for the formation of porphyry ore deposits in magmatic arcs. Nature Geoscience, 6, 917-925.

Wittenbrink, R., 1997. Zeitliche Variationen der Magmengenese miozäner bis quartärer Vulkanite im südlichen Bereich der Zentralen Vulkanischen Zone der Anden (CVZ, 20°-26°S, 67°-69°W). Berliner geowiss. Abh., Reihe A, v. 193, 135 pp.

Wood, B.J., Turner, S.P., 2009. Origin of primitive high-Mg andesite: Constraints from natural examples and experiments. Earth and Planetary Science Letters, 283, 59-66.

Yuan, X., Sobolev, S.V., Kind, R., 2002. Moho topography in the central Andes and its geodynamic implications. Earth and Planetary Science Letters, 199, 389-402.

Zajacz, Z., Candela, P.A., Piccoli, P. M., Wälle, M., Sanchez-Valle, C., 2012. Gold and copper in volatile saturated mafic to intermediate magmas: Solubilities, partitioning, and implications for ore deposit formation. Geochimica et Cosmochimica Acta, 91, 140-159.

Zandt, G., Leidig, M., Chmielowski, J., Baumont, D., Yuan, X., 2003. Seismic detection and characterization of the Altiplano-Puna magma body, Central Andes. Pure and Applied Geophysics, 160, 789-807.

Zhang, J., Humphreys, M.C., Cooper, G.F., Davidson, J.P., Macpherson, C.G., 2017. Magma mush chemistry at subduction zones, revealed by new melt major element inversion from calcic amphiboles. American Mineralogist: Journal of Earth and Planetary Materials, 102(6), 1353-1367.

Zhou, R., Schoenbohm, L.M., Cosca, M., 2013. Recent, slow normal and strikeslip faulting in the Pasto Ventura region of the Southern Puna Plateau, NW Argentina. Tectonics, 32 (1), 19-33.

Journal Pre-proof

Journal Pre-proof

FIGURE CAPTIONS

Fig. 1. A) Location of the studied monogenetic centers in the Puna plateau. B) Enlarged views in Google Earth images of the Campo Negro, Carachipampa and Pasto Ventura monogenetic centers.

Fig. 2. Classification diagrams for selected Puna amphibole-bearing mafic rocks. A) Total Alkalis vs. Silica diagram (after Le Maitre et al., 1989). B) K_2O vs. Silica (Peccerillo and Taylor, 1976).

Fig. 3. Compositional features of amphibole-bearing mafic rocks from the Puna Plateau. A) Extended multielement diagram normalized to the primitive mantle of Sun and Mcdonough (1989). B) Whole rock diagram of REE normalized to the chondrite of Sun and Mcdonough (1989). C) Whole rock Sr (μg/g) vs. MgO (wt. %) contents. D) Whole rock Y (μg/g) versus MgO (wt. %) contents.

Fig. 4. Photomicrograph of amphibole skeletal phenocrysts in the Carachipampa lava. B) Photomicrograph of the main aspect of Pasto Ventura lava samples. C) BSE image of amphibole corona around an orthopyroxene phenocryst. D) Photomicrograph of the Campo Negro lava with amphibole, plagioclase and pyroxene. E) BSE image of orthopyroxene in the core of an amphibole phenocryst. F) Typical texture of the Campo Negro basaltic enclave.

Fig. 5. A) Variation of MgO content (wt. %) from core to rim in a clinopyroxene of the Pasto Ventura lava. B) REE element composition of clinopyroxene of Southern Puna samples. Normalized to the chondrite of Sun and Mcdonough (1989).

Fig. 6. Compositions of amphiboles from Southern and Northern Puna. A) Al_2O_3 vs. TiO_2 content in weight percent. *Light grey field* corresponds to amphibole composition from Wittenbrink (1997), Lindsay (1999) and Risse (). *Dark grey field* corresponds to amphibole composition from Derruelle (1991). B) Trace element composition of amphibole from the studied samples. Normalized to the Primitive Mantle of Sun and

Mcdonough (1989). C) Sr/Y vs. TiO_2 (wt. %) values in amphibole phenocrysts. D) Amphibole REE contents normalized to the chondrite of Sun and Mcdounough (1989).

Fig. 7. A) Cu contents (μg/g) vs. TiO_2 (wt. %) for the high and low Ti-Al groups of amphibole phenocrysts. B) Correlations between Cu and Li contents (in μg/g) that follow the following linear trends: (a) Cu=1.527*Li+126.9, R=0.9; (b) Cu=4.197*Li-541.8, R=0.95; (c) Cu=4.8*Li-733.3, R=0.9; (d) Cu=1.9*Li-17, R=0.4.

Fig. 8. P-T calculations. A) Comparison of amphibole thermometers of Ridolfi et al. (2010) and Putirka (2016). Symbols as in previous figures. B, C and D) Comparison between barometers of Ridolfi and Renzulli (2012) (equations 1b, 1c, 1d) and the barometer of Putirka (2016). Symbols as in previous figures.

Fig. 9. A) K_2O vs. TiO_2 composition of amphibole. *Dashed lines* separate the compositional fields of amphibole from alkaline (A) and subalkaline (SA) series after Molina et al. (2009). B) K vs. Al composition of amphibole. *Dashed lines* separate the compositional fields of amphibole from alkaline and subalkaline series according to Ridolfi and Renzulli (2012). *Light grey field* corresponds to amphibole composition from Wittenbrink (1997), Kraemer (1999), Lindsay (1999) and Risse (2008). *Dark grey field* corresponds to amphibole composition from Derruelle (1991). C) Plot of Sr/Y vs. Y of predicted compositions of amphibole equilibrium melts (calculated by multiple regression equations according to Humphreys et al. (2019)) used to define adakite magmas (Defant and Drummond, 1990; Chiaradia et al., 2009). D) Plot of La/Yb vs. Yb from predicted compositions of amphibole equilibrium melts used to define adakite magmas (Defant and Drummond, 1990; Chiaradia et al., 2009).

Fig. 10. Bouguer gravity anomaly maps of the study areas based on the model of Prezzi et al. (2009). A) Northern Puna. B) Southern Puna. The stars indicate the location of the studied centers. CN: Campo Negro; C: Carachipampa; PV: Pasto Ventura. *Dashed line* shows the extension of the

Journal Pre-proof

Altiplano Puna Volcanic Complex (APVC).

Table 1. Bulk-rock chemical composition on anhydrous bases of the amphibole-bearing lava samples and enclave from Southern Puna (SP) and Northern Puna (NP) Neogene monogenetic centers. AN: Carachipampa. PVD: Pasto Ventura. CN09: Campo Negro.

Sample	AN-13	AN-15	PVD-6	PVD-7	PVD-8	CN09-02	CN09-11	CN09-12Mi	CN09-13	CN09-13Mi	CN09-05
Location	SP	SP	SP	SP	SP	NP	NP	NP	NP	NP	NP - enclave
Lat (S)	26.572	26.569	26.728	26.729	26.728	23.061	23.060	23.059	23.058	23.058	23.061
Long (W)	67.442	67.445	67.206	67.208	67.211	66.648	66.642	66.6[illegible]0	66.638	66.638	66.648
Mg#	62	64	60	59	61	61	62	63	62	63	65
major elements in wt.%											
SiO_2	57.04	57.48	58.02	59.50	58.31	57.37	56.72	57.74	58.39	58.09	51.02
TiO_2	1.03	0.94	1.11	1.04	1.08	1.16	1.23	1.17	1.17	1.23	2.24
Al_2O_3	13.92	13.34	13.29	13.68	13.54	15.65	16.56	15.65	15.21	15.29	15.63
Fe_2O_3	7.45	7.37	7.41	6.87	7.33	7.[illegible]7	8.21	8.03	7.98	8.12	9.47
MnO	0.11	0.11	0.11	0.11	0.12	0.11	0.11	0.10	0.10	0.11	0.11
MgO	6.19	6.48	5.65	5.06	5.68	6.18	6.12	6.12	6.03	6.34	8.99
CaO	7.95	8.10	7.88	6.91	7.2[illegible]	5.91	5.75	5.64	5.91	5.59	7.96
Na_2O	3.93	3.96	3.79	3.91	3.79	2.48	2.28	2.30	2.11	2.15	2.20
K_2O	1.98	1.84	2.25	2.45	2.38	2.84	2.68	2.91	2.78	2.74	2.15
P_2O_5	0.40	0.37	0.49	0.48	0.50	0.34	0.35	0.34	0.34	0.33	0.22
LOID	1.12	1.24	1.20	1.49	1.39	0.51	1.20	0.70	1.60	1.10	0.65
total	100.42	100.10	100.45	100.78	100.97	100.00	100.00	100.00	100.00	100.00	98.80
trace elements in µg/g											
Cu		54			37						25
Ba	645	602	683	754	730	884	879	930	939	872	558
Sr	906	910	805	818	807	480	495	481	579	491	523
Rb	51	50	59	68	63	112	108	122	99	110	68
Cs	2	2	3	3	3	11	12	20		18	6
Nb	13	11	18	18	20	19	20	19	17	20	16

Ta	0.7	0.6	0.9	1.0	1.1	1.6	1.6	1.6		1.6	1.1
Zr	180	172	215	213	218	203	216	200	257	188	148
Y	19	19	21	21	21	25	26	26	25	27	43
Cr	295	350	298	239	259	384	365	387	359	391	570
Ni	128	138	85	81	88	89	47	121	64	108	126
La	69	66	58	62	63	45	50	46		46	40
Ce	130	125	110	115	117	85	94	87		94	84
Pr	13	13	11	12	12	10	11	11		10	10
Nd	49	49	43	45	47	37	41	[illegible]		40	44
Sm	7.7	7.9	7.0	7.5	7.7	7.1	7.7	7.4		7.6	9.3
Eu	2.0	1.9	1.8	1.9	1.9	1.7	1.9	1.8		1.8	2.3
Gd	6.4	5.8	6.2	6.0	6.3	5.8	6.1	6.1		6.3	10.2
Tb	0.7	0.7	0.7	0.7	0.7	0.8	0.9	0.9		0.9	1.4
Dy	3.9	3.7	3.8	4.0	4.0	4.4	4.7	4.7		5.4	7.7
Ho	0.7	0.7	0.7	0.8	0.8	0.9	0.9	0.9		1.0	1.4
Er	1.9	1.9	2.1	1.9	2.3	2.3	2.5	2.5		2.7	4.0
Tm	0.2	0.2	0.2	0.3	0.3	0.4	0.4	0.4		0.4	0.5
Yb	1.8	1.9	1.8	1.8	[illegible]	2.2	2.4	2.3		2.5	3.5
Lu	0.3	0.3	0.3	0.3	0.3	0.4	0.4	0.4		0.4	0.5
Hf	5	5	6	6	6	5	6	5	5	6	4
Th	10	9	11	12	12	12	13	12		11	7
U	2	2	3	3	3	3	3	3		3	2

*Total iron expressed as Fe_2O_3

Table 2. Chemical composition of representative anhydrous mineral phenocrysts in the amphibole-bearing lava samples and enclave from Southern and Northern Puna Neogene monogenetic centers.

Site	Pasto Ventura	Carachipampa	Campo Negro

Sample	PVD6		PVD7	PVD8	AN13		AN15		CN09-2		CN09-5	
Mineral	Ol	Cpx	Cpx	Cpx	Ol	Cpx	Ol	Cpx	Opx	Pl	Opx	Pl
SiO_2	37.93	51.18	51.20	50.88	39.38	50.51	39.07	47.99	55.63	48.00	54.00	49.54
TiO_2	0.09	1.08	0.91	1.11	0.06	0.71	0.00	1.48	0.20		0.33	0.01
Al_2O_3	0.00	4.62	3.39	3.48	0.02	4.28	0.02	5.74	2.08	32.94	3.53	32.34
Cr_2O_3	0.00	0.22	0.09	0.00	0.01	0.14	0.03	0.08	0.64		0.88	
NiO	0.18				0.30		0.28					
FeO	16.56	5.81	7.01	8.58	14.59	7.31	15.14	8.39	7.56	0.26	8.15	0.23
MnO		0.04	0.17	0.28		0.21		0.18	0.16		0.14	0.01
MgO	44.93	14.48	15.84	15.56	45.58	15.81	45.45	14.49	32.96		31.89	0.05
CaO	0.02	21.91	20.73	19.85	0.11	20.22	0.09	20.92	0.94	15.54	1.14	14.63
Na_2O		0.68	0.47	0.37		0.58		0.36	0.02	2.39	0.04	2.73
K_2O										0.16		0.27
Total	99.71	100.02	99.81	100.11	100.05	99.76	100.08		100.18	99.30	100.10	99.98
An										78		75
Ab										22		25
Fs		47	43	41		42		44	2		2	
Wo		10	12	14		12		14	11		12	
En		43	46	45		46		42	87		85	
Fo	83				83		84					
Cr#												
Mg#		84	85	81		87		86	89			

Ol olivine, *Cpx* clinopyroxene, *Opx* orthopyroxene, *Pl* plagioclase.

Data are single point analyses of phenocryst cores.

Table 3. Representative major element composition of amphibole phenocrysts in the amphibole-bearing lava samples and enclave from Southern and Northern Puna Neogene monogenetic centers.

Sample	PVD6	PVD6	PVD6	PVD6	PVD7	PVD7	PVD8	PVD8	PVD8	PVD8

Grain	6-2	6-2	19-1	19-1	16-1	16-1	8-1	8-1	16-1	16-1
Position	c	r	c	r	c	r	c	r	c	r
F	0.00	0.00	0.00	0.00	0.00	0.00	0.00	0.00	0.00	0.00
Cl	0.03	0.03	0.03	0.03	0.04	0.03	0.03	0.03	0.04	0.03
SiO_2	42.28	43.22	42.87	42.67	41.75	43.10	43.39	44.07	42.88	44.06
Al_2O_3	11.86	10.84	11.94	11.74	12.69	11.85	13.09	12.23	12.86	11.12
K_2O	0.91	0.87	0.96	0.94	0.93	0.85	1.02	0.93	0.92	0.83
TiO_2	2.72	2.64	2.54	2.71	2.68	2.53	2.59	2.41	3.00	2.60
Cr_2O_3	0.10	0.15	0.15	0.15	0.12	0.07	0.07	0.17	0.06	0.15
CaO	11.11	11.40	11.00	11.31	11.06	11.05	10.86	10.97	10.68	11.22
BaO	0.13	0.12	0.04	0.06	0.19	0.17	0.13	0.08	0.17	0.19
Na_2O	2.37	2.25	2.38	2.37	2.52	2.34	2.51	2.45	2.37	2.26
MgO	15.91	16.08	15.14	16.27	14.84	15.97	15.77	16.71	13.86	16.32
FeO	9.49	9.57	10.40	8.65	10.62	9.65	9.08	8.24	11.52	9.04
MnO	0.10	0.11	0.13	0.12	0.14	0.13	0.12	0.10	0.11	0.11
Total	97.00	97.27	97.59	97.02	97.58	97.74	98.67	98.39	98.47	97.93

Sample	AN13	AN13	AN13	AN13	AN15	AN15	AN15	AN15
Grain	1-1	1-1	2-2	2-2	4-6	4-6	8-4	8-4
Position	c	r	c	r	c	r	c	r
F	0.03	0.00	0.02	0.02	0.00	0.00	0.06	0.02
Cl	0.04	0.03	0.04	0.03	0.03	0.03	0.03	0.02
SiO_2	43.73	42.68	42.59	42.97	42.24	42.83	42.54	42.79
Al_2O_3	11.50	12.14	12.45	12.23	12.53	12.34	12.16	12.37
K_2O	0.64	0.70	0.71	0.68	0.65	0.72	0.70	0.71

Journal Pre-proof

TiO_2	3.08	2.96	2.92	3.00	2.87	2.68	2.62	2.64
Cr_2O_3	0.05	0.15	0.15	0.16	0.31	0.34	0.38	0.35
CaO	11.86	11.89	11.77	11.88	11.75	11.76	11.81	11.57
BaO	0.09	0.06	0.12	0.13	0.18	0.17	0.16	0.14
Na_2O	2.28	2.27	2.38	2.41	2.30	2.35	2.31	2.25
MgO	16.19	15.77	15.87	15.94	15.89	16.17	16.27	16.23
FeO	9.79	9.88	9.84	9.99	9.72	9.02	8.98	9.09
MnO	0.12	0.08	0.12	0.11	0.11	0.07	0.10	0.12
Total	99.40	98.63	98.97	99.54	98.56	98.78	98.12	98.31

Sample	CN09-2	CN09-2	CN09-2	CN09-2	CN09-5	CN09-5	CN09-5	CN09-5
Grain	14-2	14-2	15-1	15-1	6-2	6-2	15-1	15-1
Position	c	r	c	r	c	r	c	r
F	0.02	0.00	0.02	0.00	0.06	0.02	0.00	0.00
Cl	0.04	0.04	0.02	0.03	0.04	0.03	0.04	0.03
SiO_2	39.89	40.33	41.47	41.51	41.43	41.76	41.95	42.37
Al_2O_3	14.04	13.67	14.01	14.19	13.90	14.03	13.63	13.74
K_2O	1.40	1.37	1.20	1.20	1.28	1.31	1.28	1.26
TiO_2	3.54	3.19	2.97	3.08	3.89	4.16	3.45	4.03
Cr_2O_3	0.09	0.06	0.06	0.00	0.11	0.11	0.18	0.23
CaO	11.61	11.54	11.51	11.45	11.51	11.57	11.59	11.72
BaO	0.14	0.21	0.09	0.20	0.15	0.11	0.18	0.17
Na_2O	1.93	1.88	2.11	2.11	1.86	1.89	1.90	1.91
MgO	15.05	14.64	15.53	14.82	14.51	13.87	14.36	14.10
FeO	9.48	10.03	9.25	9.95	9.93	10.28	10.12	9.56

MnO	0.10	0.12	0.09	0.09	0.10	0.14	0.14	0.09
Total	97.33	97.09	98.35	98.63	98.78	99.29	98.82	99.20

c core, *r* rim.

Data are single point analyses of phenocryst.

Table 4. Representative LA-ICPMS analyses of trace element composition of amphibole phenocrysts.

Sample	PVD8	PVD8	PVD8	PVD8	AN15	AN15	AN15	CN09-5	CN09-5	CN09-5	CN09-5
Grain	8-1	8-1	16-1	16-1	4-6	8-4	8-4	6-2	6-2	15-1	15-1
Position	c	r	c	r	c	c	r	c	r	c	r
Cu	52	13	23	52	206	73	343	4		4	4
Li	139	133	146	195	191	[illegible]	145	46	48	55	47
Sr	411	366	341	353	[illegible]	577	539	416	357	418	394
Rb	4.10	4.17	4.22	4.47	[illegible]	2.55	2.55	8.01	7.22	8.57	7.78
Nb	45	47	6	11	6	6	6	12	14	11	12
Ta	0.27	0.24	0.33	[illegible]	0.30	0.32	0.28	0.59	0.66	0.59	0.64
Zr	6.31	5.51	46.24	[illegible]	71.53	68.71	63.21	70.99	67.34	65.74	59.72
Hf	2.07	1.82	2.08	[illegible]		3.29	2.97	3.31	3.07	3.10	2.89
Y	17.18	16.27	[illegible]	30.01	28.39	28.66	27.40	47.02	45.04	51.33	41.55
Ni	353	349	345	232	367	6	6	78	86	83	82
La	7.25	6.21	5.63	9.51	11.22	12.64	11.80	12.62	11.22	13.33	10.93
Ce	27.68	22.92	20.70	35.94	40.99	45.06	41.99	46.95	41.82	47.23	39.23
Pr	4.42	4.08	3.79	6.41	7.26	7.88	7.20	8.32	7.61	8.40	7.26
Nd	23.61	22.29	21.20	32.68	38.47	42.88	39.84	46.62	40.81	44.67	38.96
Sm	6.29	5.98	5.70	8.70	9.92	10.45	10.45	13.27	11.71	12.70	11.34
Eu	1.84	1.70	1.73	2.31	2.69	2.77	2.57	2.97	2.56	2.96	2.73

Gd	5.59	5.56	5.22	8.00	9.23	9.22	9.05	12.78	11.37	13.22	11.50
Tb	0.71	0.64	0.72	1.10	1.19	1.20	1.17	1.73	1.70	1.87	1.61
Dy	4.02	3.79	3.81	6.18	6.50	6.71	6.13	10.30	9.93	10.08	9.10
Ho	0.70	0.72	0.71	1.12	1.16	1.16	1.12	1.89	1.79	2.00	1.64
Er	1.83	1.65	1.72	3.09	3.01	2.92	2.83	5.10	4.77	4.87	4.29
Tm			0.24	0.41	0.35	0.37	0.34	0.62	0.60	0.63	0.54
Yb	1.15	1.09	1.32	2.32	2.10	2.13	2.07	3.59	3.62	3.58	3.10
Lu				0.34	0.29	0.31	0.30	0.49	0.46	0.49	0.41
Pb	4.69	0.74	0.84	3.63	0.86	0.81	0.85	1.47	1.30	1.40	1.26

c core, *r* rim.

Data are single point analyses of phenocryst.

Table 5. Conditions of crystallization for selected amphiboles.

Sample	Grain	Temperature (°C)		Pressure (kbar)						ln fO_2 (ΔNNO)	Melt H_2O (wt. %)	Melt SiO_2 (wt. %)
		R10	P16	R10	RR12 (1a)	RR12 (1b)	RR12 (1c)	RR12 (1d)	P16	R10	R10	RR12
PVD6	6-1	995	981	3.9	7.[illegible]	4.2	4.7	8.2	3.8	1.6	5	65
PVD7	9-2	975	962	4.0	6.0	4.1	4.4	6.4	5.6	1.1	5	64
AN13	16-1	1006	1006	4.0	6.4	4.4	4.9	5.7	5.8	1.1	5	59
AN13	20-2	1008	1006	4.1	5.4	4.3	4.7	4.8	5.0	1.2	5	58
AN15	1-1	996	991	4.0	5.7	4.3	4.8	5.2	5.3	1.3	5	60
AN15	12-1	989	985	3.9	5.1	4.1	4.5	5.1	4.8	1.1	5	61
CN09-2	2-1	1013	998	5.5	7.0	6.2	5.9	6.1	6.4	0.7	5	56
CN09-2	2-1	1006	994	4.8	6.1	5.4	5.5	5.4	5.8	0.7	5	58
CN09-5	5-1	1024	1008	6.0	6.8	6.5	5.9	6.1	6.4	0.5	5	55
CN09-5	6-2	1015	1000	5.6	6.3	6.2	5.8	5.2	6.0	0.6	5	55

R10 = values calculated with the equations of Ridolfi et al. (2010); RR12 = values calculated with the equations of Ridolfi and Renzulli (2012); P16 = values calculated with the

Journal Pre-proof

equations of Putirka (2016).

Table 6. Conditions of crystallization for selected olivine, clinopyroxene, orthopyroxene and plagioclase. Temperature in °C and pressure in kbar.

Sample	**Putirka et al. (2007)**			**Putirka (2008)**		
	Eq. 4	**Eq. 32c**	**Eq. 33**	**Eq. 28a**	**Eq. 29b**	**Eq. 24a**
	T_{ol}	P_{cpx}	T_{cpx}	T_{opx}	P_{opx}	T_{pl}
AN13	1135	11	1150			
AN15	1140	10	1145			
PVD6		11	1150			
PVD7		10	1140			
PVD8		10	1175			
CN09-2				1185	9	1120
CN09-5				1212	10	1150

Declaration of interests

☒ The authors declare that they have no known competing financial interests or personal relationships that could have appeared to influence the work reported in this paper.

☐The authors declare the following financial interests/personal relationships which may be considered as potential competing interests:

HIGHLIGHTS

- Few monogenetic centers of the Puna produced mafic rocks with amphibole phenocrysts.

Journal Pre-proof

- Amphiboles are compositionally diverse between Southern and Northern Puna.
- Chemical contrasts reveal high vs low pressure differentiation of hydrous magmas.
- High concentration of Cu during amphibole crystallization in the Southern Puna.

Journal Pre-proof

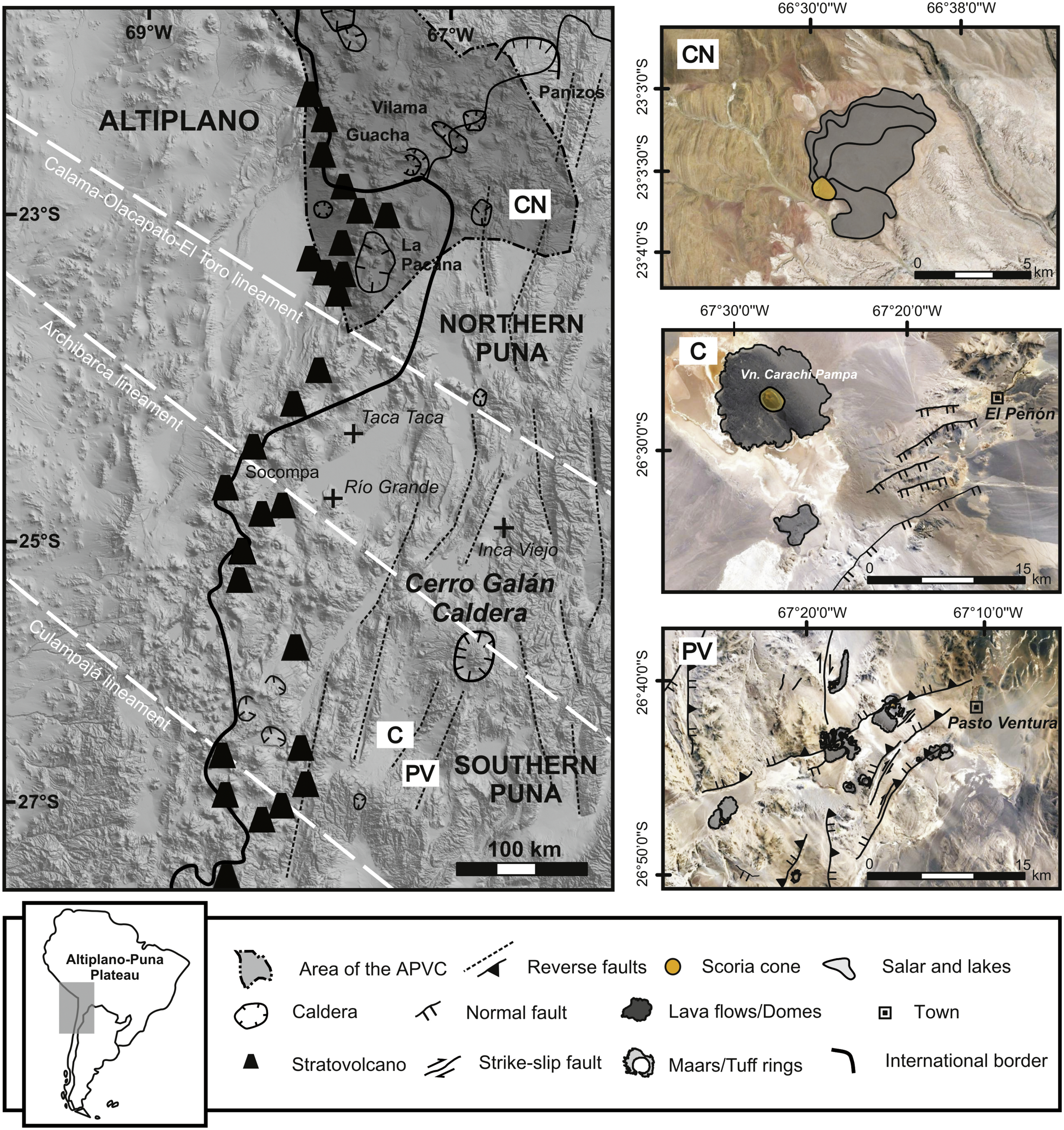
69°W
67°W
ALTIPLANO
Vilama
Guacha
Panizos
CN
La Pacana
23°S
25°S
27°S
Calama-Olacapato-El Toro lineament
Archibarca lineament
Culampajá lineament
NORTHERN PUNA
Taca Taca
Socompa
Río Grande
Inca Viejo
Cerro Galán Caldera
C
PV
SOUTHERN PUNA
100 km
66°30'0"W
66°38'0"W
23°3'0"S
23°3'30"S
23°4'0"S
0
5
km
67°30'0"W
67°20'0"W
Vn. Carachi Pampa
El Peñón
26°30'0"S
15
67°10'0"W
26°40'0"S
26°50'0"S
Pasto Ventura
Altiplano-Puna Plateau
Area of the APVC
Reverse faults
Scoria cone
Salar and lakes
Caldera
Normal fault
Lava flows/Domes
Town
Stratovolcano
Strike-slip fault
Maars/Tuff rings
International border

Figure 1

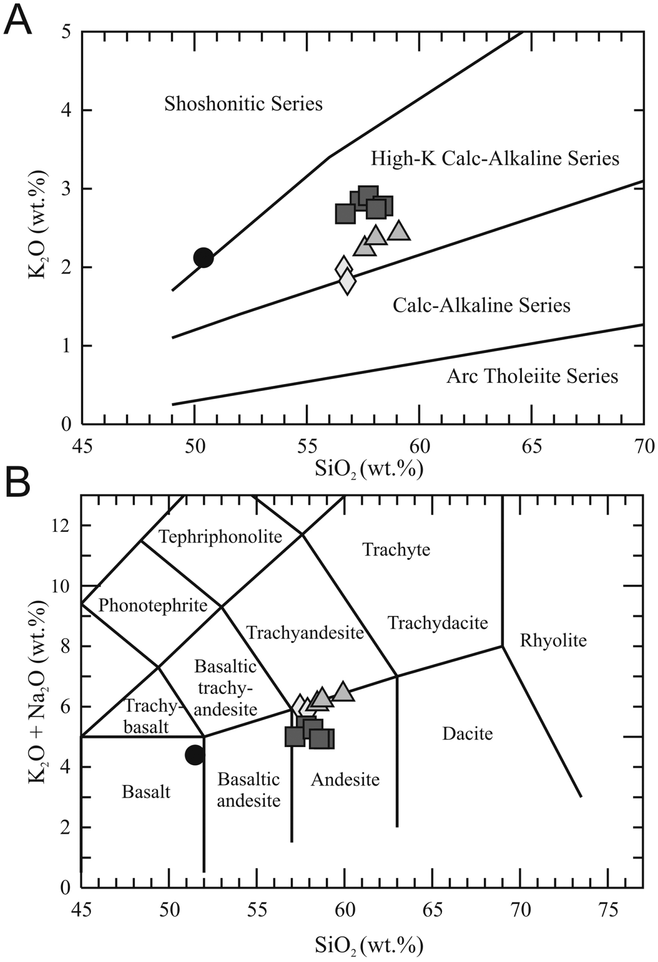
A
Shoshonitic Series
High-K Calc-Alkaline Series
Calc-Alkaline Series
Arc Tholeiite Series
K_2O (wt.%)
SiO_2 (wt.%)
B
Tephriphonolite
Trachyte
Phonotephrite
Trachyandesite
Trachydacite
Rhyolite
Basaltic trachy- andesite
Trachy- basalt
Dacite
Basalt
Basaltic andesite
Andesite
$K_2O + Na_2O$ (wt.%)
SiO_2 (wt.%)

Figure 2

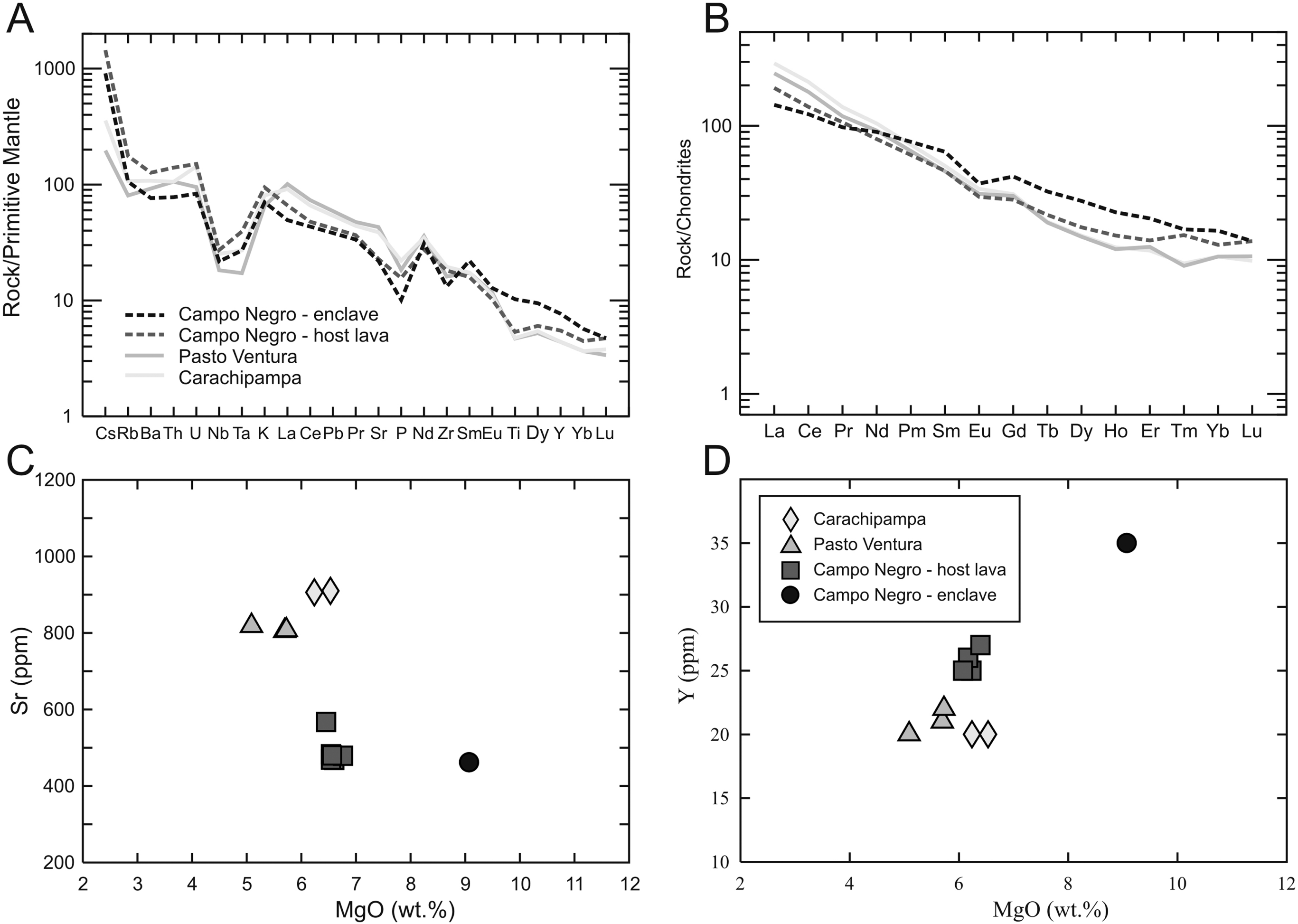
A
B
C
D
Rock/Primitive Mantle
1000
100
10
1
Cs Rb Ba Th U Nb Ta K La Ce Pb Pr Sr P Nd Zr Sm Eu Ti Dy Y Yb Lu
Campo Negro - enclave
Campo Negro - host lava
Pasto Ventura
Carachipampa
Rock/Chondrites
La Ce Pr Nd Pm Sm Eu Gd Tb Dy Ho Er Tm Yb Lu
Sr (ppm)
1200
1000
800
600
400
200
2 3 4 5 6 7 8 9 10 11 12
MgO (wt.%)
Y (ppm)
35
30
25
20
15
10
2 4 6 8 10 12
Carachipampa
Pasto Ventura
Campo Negro - host lava
Campo Negro - enclave

Figure 3

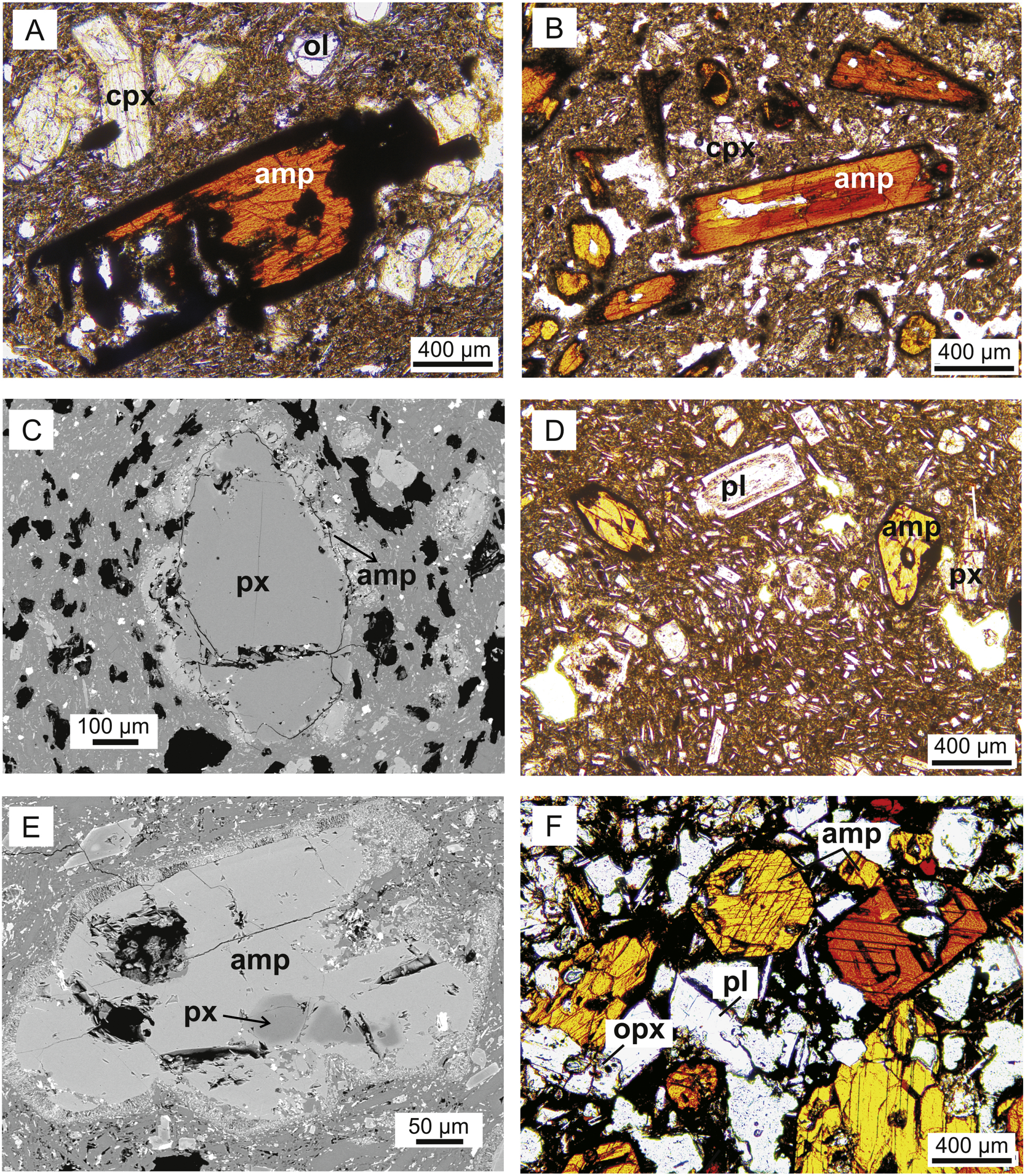
A
ol
cpx
amp
400 µm
B
cpx
amp
400 µm
C
px
amp
100 µm
D
pl
amp
px
400 µm
E
amp
px
50 µm
F
amp
pl
opx
400 µm

Figure 4

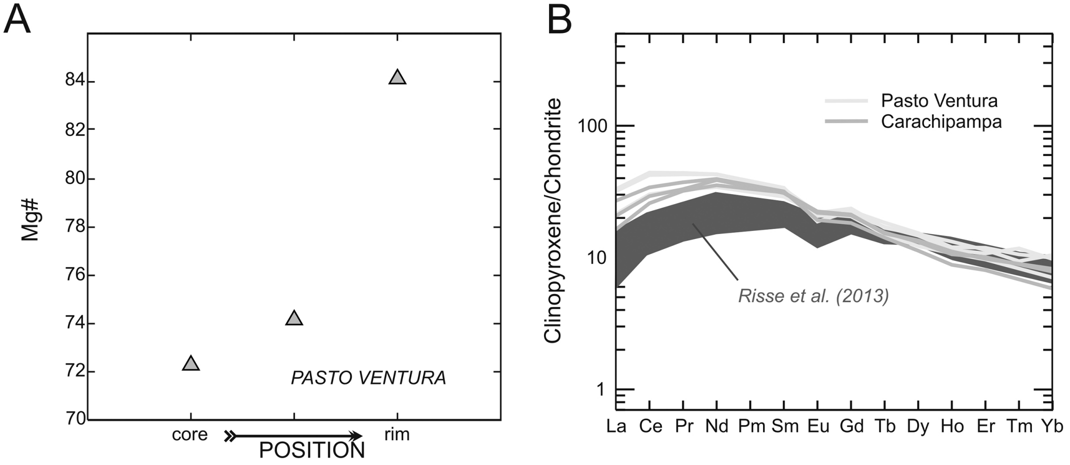
A
Mg#
84
82
80
78
76
74
72
70
PASTO VENTURA
core
rim
POSITION
B
Clinopyroxene/Chondrite
100
10
1
Pasto Ventura
Carachipampa
Risse et al. (2013)
La
Ce
Pr
Nd
Pm
Sm
Eu
Gd
Tb
Dy
Ho
Er
Tm
Yb

Figure 5

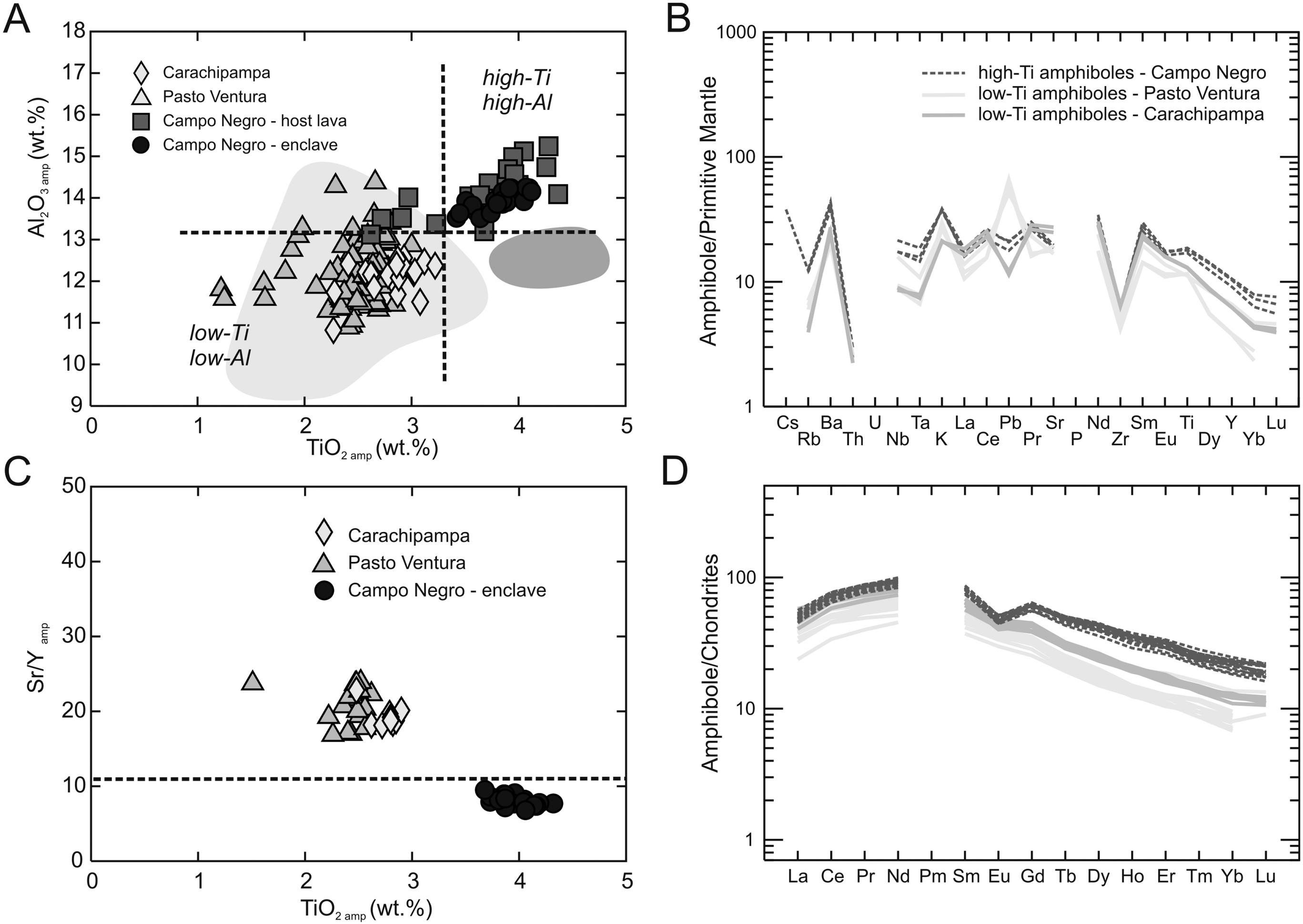
A
B
C
D
Carachipampa
Pasto Ventura
Campo Negro - host lava
Campo Negro - enclave
high-Ti
high-Al
low-Ti
low-Al
$Al_2O_{3\ amp}$ (wt.%)
$TiO_{2\ amp}$ (wt.%)
high-Ti amphiboles - Campo Negro
low-Ti amphiboles - Pasto Ventura
low-Ti amphiboles - Carachipampa
Amphibole/Primitive Mantle
Cs Rb Ba Th U Nb Ta K La Ce Pb Pr Sr P Nd Zr Sm Eu Ti Dy Y Yb Lu
Sr/Y_{amp}
Amphibole/Chondrites
La Ce Pr Nd Pm Sm Eu Gd Tb Dy Ho Er Tm Yb Lu

Figure 6

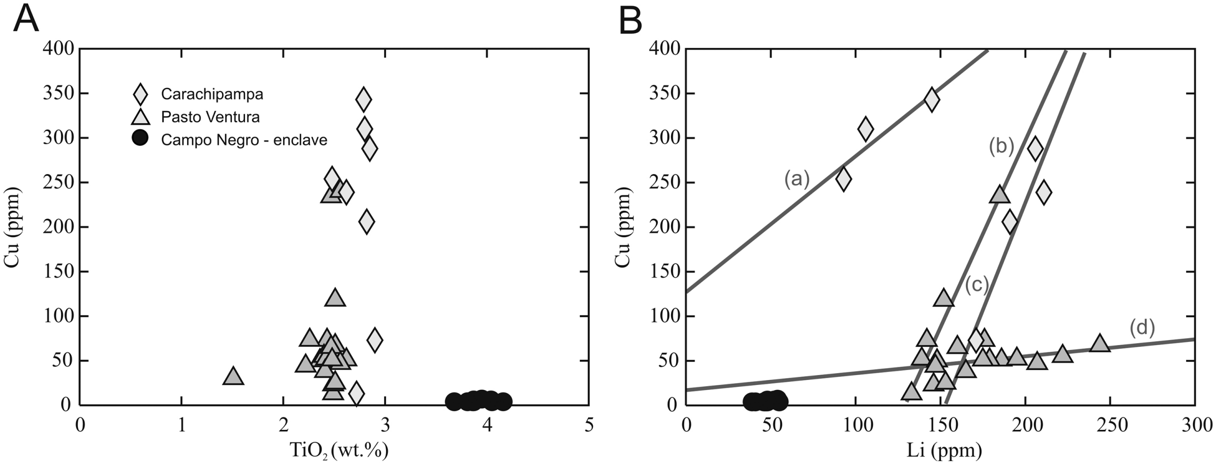

A
B
400
350
300
250
200
150
100
50
0
Cu (ppm)
0
1
2
3
4
5
TiO$_2$ (wt.%)
Carachipampa
Pasto Ventura
Campo Negro - enclave
(a)
(b)
(c)
(d)
50
100
150
200
250
300
Li (ppm)

Figure 7

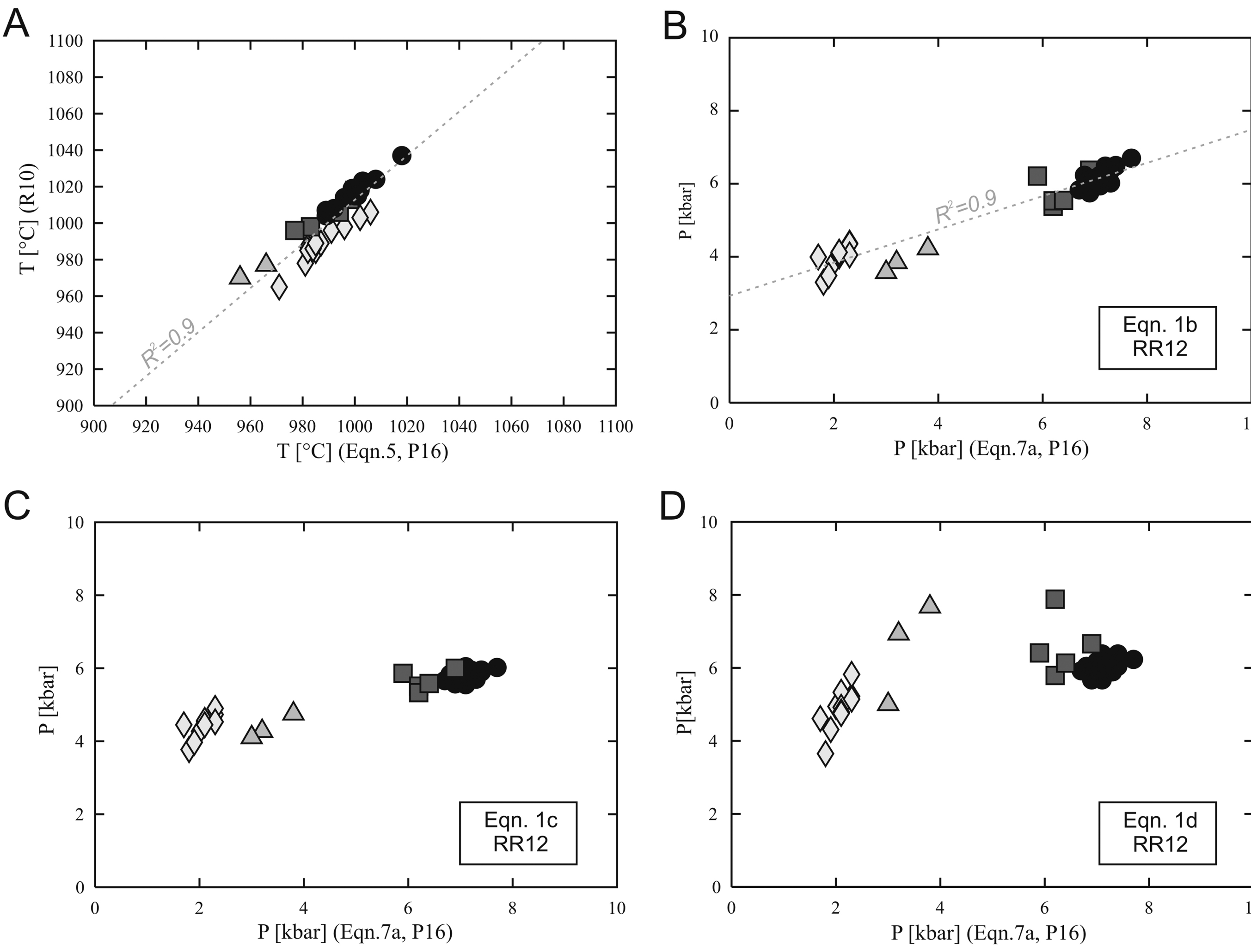

A
T [°C] (R10)
T [°C] (Eqn.5, P16)
R^2=0.9
B
P [kbar]
P [kbar] (Eqn.7a, P16)
R^2=0.9
Eqn. 1b
RR12
C
P [kbar]
P [kbar] (Eqn.7a, P16)
Eqn. 1c
RR12
D
P[kbar]
P [kbar] (Eqn.7a, P16)
Eqn. 1d
RR12

Figure 8

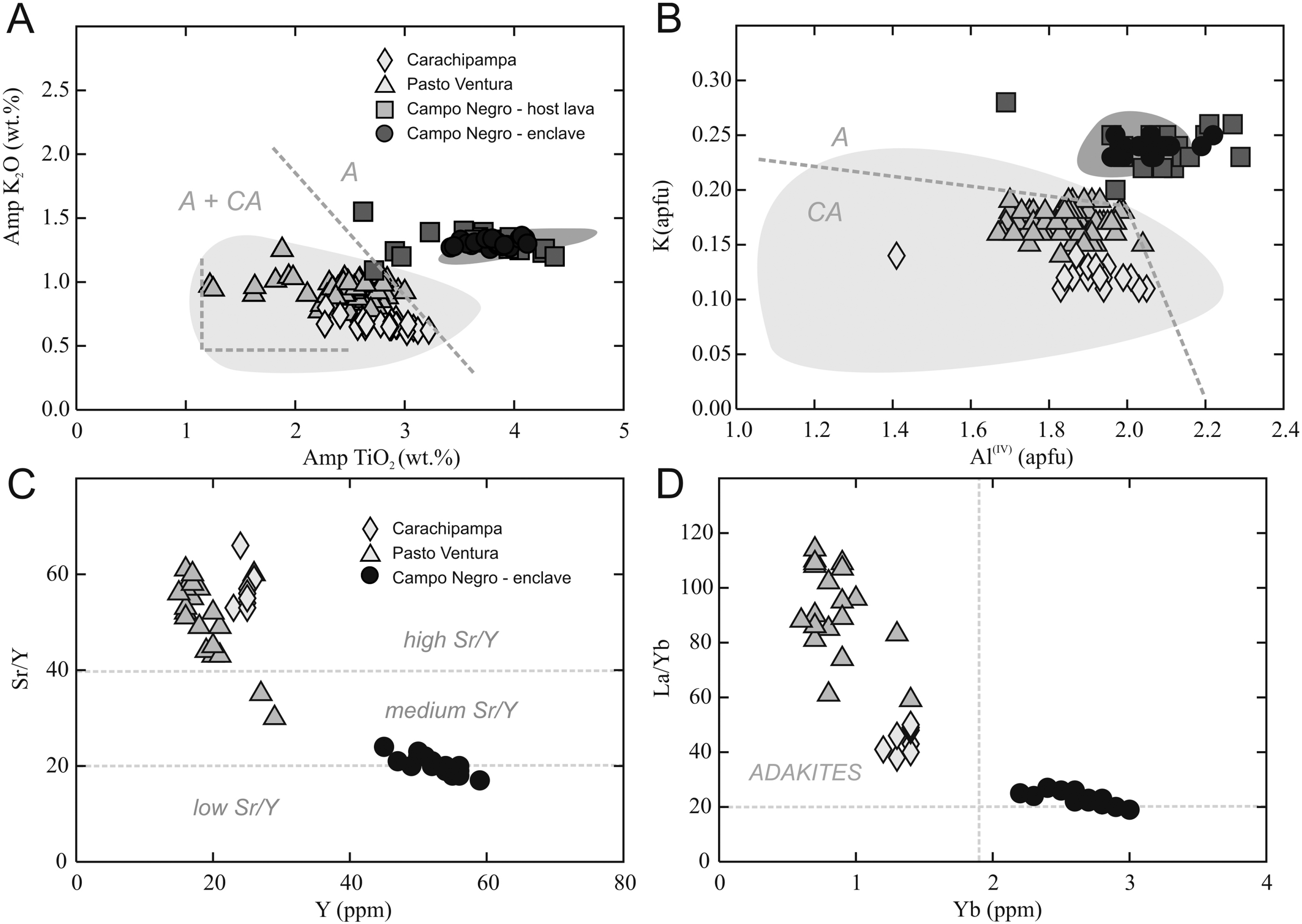
A
Carachipampa
Pasto Ventura
Campo Negro - host lava
Campo Negro - enclave
A + CA
A
Amp K_2O (wt.%)
Amp TiO_2 (wt.%)
B
A
CA
K(apfu)
$Al^{(IV)}$ (apfu)
C
Carachipampa
Pasto Ventura
Campo Negro - enclave
high Sr/Y
medium Sr/Y
low Sr/Y
Sr/Y
Y (ppm)
D
ADAKITES
La/Yb
Yb (ppm)

Figure 9

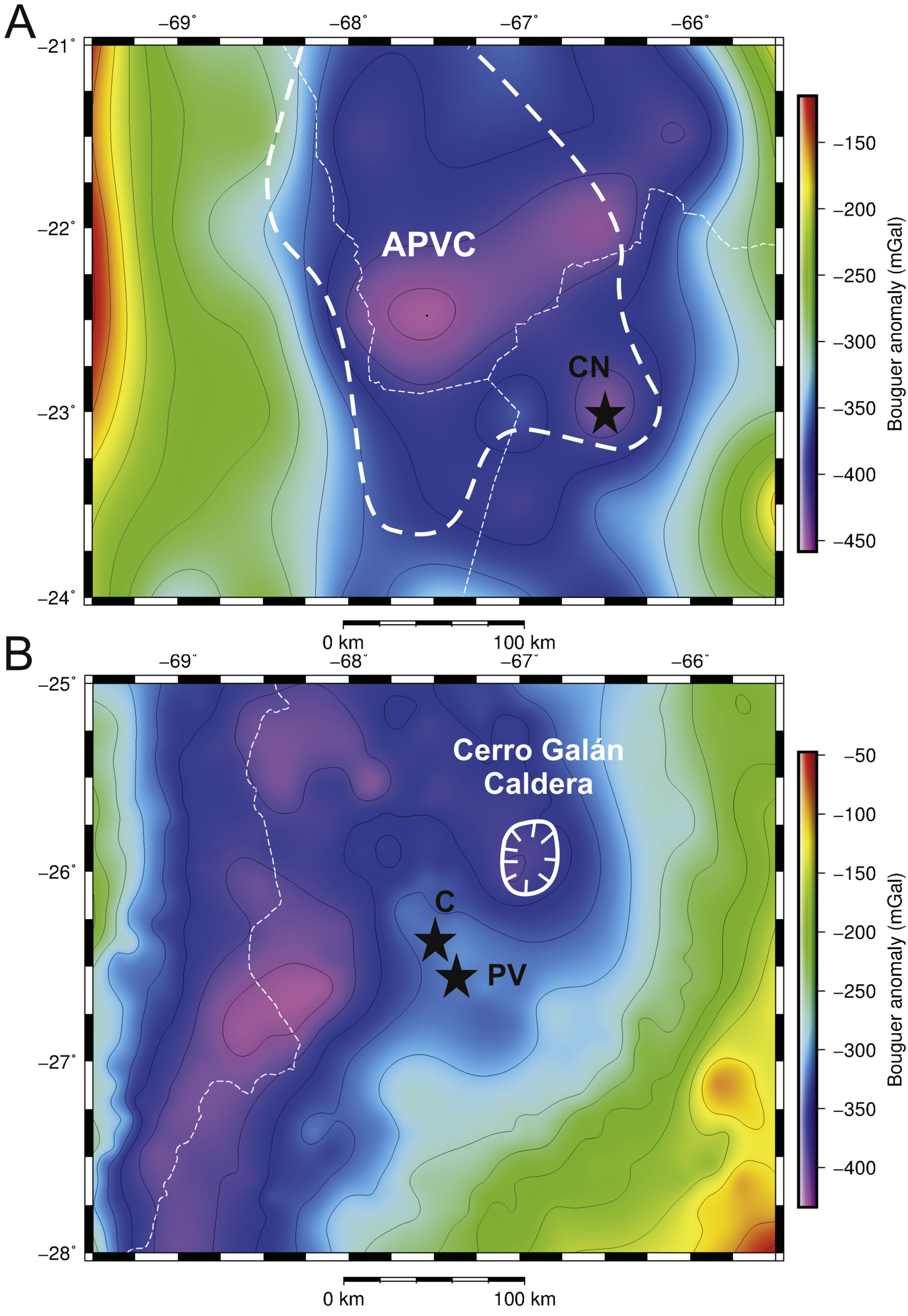
A
−69˚
−68˚
−67˚
−66˚
−21˚
−22˚
−23˚
−24˚
APVC
CN
−150
−200
−250
−300
−350
−400
−450
Bouguer anomaly (mGal)
0 km
100 km
B
−69˚
−68˚
−67˚
−66˚
−25˚
−26˚
−27˚
−28˚
Cerro Galán
Caldera
C
PV
−50
−100
−150
−200
−250
−300
−350
−400
Bouguer anomaly (mGal)
0 km
100 km

Figure 10